

RESEARCH ARTICLE

Physiological and genomic evidence that selection on the transcription factor *Epas1* has altered cardiovascular function in high-altitude deer mice

Rena M. Schweizer¹*, Jonathan P. Velotta¹, Catherine M. Ivy², Matthew R. Jones¹, Sarah M. Muir², Gideon S. Bradburd³, Jay F. Storz⁴, Graham R. Scott², Zachary A. Cheviron¹

1 Division of Biological Sciences, University of Montana, Missoula, Montana, United States of America, **2** Department of Biology, McMaster University, Hamilton, ON, Canada, **3** Ecology, Evolutionary Biology, and Behavior Graduate Group, Department of Integrative Biology, Michigan State University, East Lansing, Michigan, United States of America, **4** School of Biological Sciences, University of Nebraska, Lincoln, Nebraska, United States of America

* These authors contributed equally to this work.

* rena.schweizer@umontana.edu



OPEN ACCESS

Citation: Schweizer RM, Velotta JP, Ivy CM, Jones MR, Muir SM, Bradburd GS, et al. (2019) Physiological and genomic evidence that selection on the transcription factor *Epas1* has altered cardiovascular function in high-altitude deer mice. *PLoS Genet* 15(11): e1008420. <https://doi.org/10.1371/journal.pgen.1008420>

Editor: Anna Di Rienzo, University of Chicago, UNITED STATES

Received: April 24, 2019

Accepted: September 13, 2019

Published: November 7, 2019

Copyright: © 2019 Schweizer et al. This is an open access article distributed under the terms of the [Creative Commons Attribution License](https://creativecommons.org/licenses/by/4.0/), which permits unrestricted use, distribution, and reproduction in any medium, provided the original author and source are credited.

Data Availability Statement: Sequencing reads from exome capture and TagSeq are available as de-multiplexed raw FASTQ files on the NCBI Short Read Archive (PRJNA528923). Additional materials are available within the Supporting Information.

Funding: Funding support was provided by the National Science Foundation (<https://nsf.gov/>); OIA 1736249 to ZAC and JFS; IOS 1755411 to ZAC and GRS; Postdoctoral Research Fellowship in Biology 1612859 to RMS), the National Heart, Lung, and

Abstract

Evolutionary adaptation to extreme environments often requires coordinated changes in multiple intersecting physiological pathways, but how such multi-trait adaptation occurs remains unresolved. Transcription factors, which regulate the expression of many genes and can simultaneously alter multiple phenotypes, may be common targets of selection if the benefits of induced changes outweigh the costs of negative pleiotropic effects. We combined complimentary population genetic analyses and physiological experiments in North American deer mice (*Peromyscus maniculatus*) to examine links between genetic variation in transcription factors that coordinate physiological responses to hypoxia (hypoxia-inducible factors, HIFs) and multiple physiological traits that potentially contribute to high-altitude adaptation. First, we sequenced the exomes of 100 mice sampled from different elevations and discovered that several SNPs in the gene *Epas1*, which encodes the oxygen sensitive subunit of HIF-2 α , exhibited extreme allele frequency differences between highland and lowland populations. Broader geographic sampling confirmed that *Epas1* genotype varied predictably with altitude throughout the western US. We then discovered that *Epas1* genotype influences heart rate in hypoxia, and the transcriptomic responses to hypoxia (including HIF targets and genes involved in catecholamine signaling) in the heart and adrenal gland. Finally, we used a demographically-informed selection scan to show that *Epas1* variants have experienced a history of spatially varying selection, suggesting that differences in cardiovascular function and gene regulation contribute to high-altitude adaptation. Our results suggest a mechanism by which *Epas1* may aid long-term survival of high-altitude deer mice and provide general insights into the role that highly pleiotropic transcription factors may play in the process of environmental adaptation.

Blood Institute of the National Institutes of Health (<https://www.nhlbi.nih.gov/>); HL087216 to JFS; Research Service Award Fellow to JPV, Grant Number 1F32HL136124-01, and the Natural Sciences and Engineering Research Council of Canada (http://www.nserc-crsng.gc.ca/index_eng.asp); Discovery Grant 418202-2012 to GRS; Postgraduate Scholarship to CMI). The funders had no role in study design, data collection and analysis, decision to publish, or preparation of the manuscript.

Competing interests: The authors have declared that no competing interests exist.

Author summary

Adaptation often requires coordinated evolutionary changes across multiple dynamic systems to maintain physiological function. For example, high-altitude habitats place a premium on tissue-oxygen delivery to cope with limited oxygen availability (hypoxia). Circulatory O₂ transport is regulated dynamically, changing on the order of seconds, and results from several interacting physiological processes. The mechanisms of adaptation in such complex phenotypes are poorly understood. One promising candidate is the gene *Epas1*, which encodes a transcription factor that regulates physiological responses to hypoxia. We used population genomic analyses and physiological assays to explore the connections between *Epas1* genetic variation and physiological function in high-altitude deer mice, which exhibit evolutionary adaptations to hypoxia. We identified a mutation in *Epas1* that is associated with variation in cardiovascular function: the predominant variant at high altitude is associated with the maintenance of an elevated heart rate under hypoxia and with differences in the expression of genes that influence heart rate and are regulated by *Epas1*. Our population genomic analyses demonstrated that *Epas1* exhibits a signature of natural selection at high altitude, suggesting that these phenotypic effects influence Darwinian fitness. Our results suggest that adaptation in complex and dynamic traits may be attributable to relatively simple genetic changes.

Introduction

Adaptive evolution often involves changes in multiple phenotypes across interacting biological pathways. How such multi-trait adaptations are produced by natural selection is an open question that requires connecting genetic variation to organismal function and fitness [1]. One promising mechanism involves functional modification of transcription factors. Because transcription factors coordinate the expression of suites of genes, they may allow for the simultaneous alteration of multiple phenotypes, making them common targets of selection [2–4]. However, mutational changes in transcription factors often have negative pleiotropic effects, which may limit the role of such changes in environmental adaptation [5,6]. If pleiotropic constraints are common, then mutations in downstream target genes may be expected to play a more prominent role in local adaptation [5,6].

Animals adapted to high-altitude (>3,000 m a.s.l.) [7] represent a unique system to understand the role of transcription factors in multi-trait adaptation. Coping with extreme hypoxia (low O₂ availability) and cold requires coordinated changes in interacting physiological pathways [8–10], including steps of the O₂ transport cascade that ensure O₂ supply matches demand. Many of these responses to hypoxia are coordinated by a single family of transcription factors, the hypoxia inducible factors (HIF 1–3) [11]. In particular, the gene *Epas1*, which encodes the O₂-sensitive α subunit of HIF-2, has been the repeated target of selection in indigenous high-altitude human and non-human populations [8,12–15]. In many ways, this pattern of repeated selection is surprising: although acute activation of HIFs lead to beneficial changes in O₂ homeostasis (e.g. *via* ventilatory acclimatization [16] and angiogenesis [17]), chronic HIF activity is often linked to high-altitude disease [10]. Thus, modification of HIF signaling may be constrained by antagonistic pleiotropy.

Determining the extent of pleiotropic constraint requires an understanding of the phenotypic effects of naturally segregating HIF variants. Studies in indigenous Tibetan humans, for example, have linked allelic variation at *Epas1* to the maintenance of normal blood

hemoglobin content [8,13] and blood concentrations of erythropoietin (which stimulates red blood cell production) under conditions of environmental hypoxia [18]. This maintenance of hemoglobin content under hypoxia is also associated with a missense variant in *Egln1* that covaries with *Epas1* genotype in Tibetans [18] and promotes HIF degradation under hypoxia [19]. However, follow-up studies found that *Epas1* genotype did not have a statistically significant influence on breathing or pulmonary function within Tibetans living at low elevation, although there were pronounced differences in several cardiorespiratory phenotypes between Tibetans and Han Chinese [18]. Nevertheless, a range of other respiratory and cardiovascular system responses to chronic hypoxia are influenced by HIF-2 signaling, including the hypoxic ventilatory response [16,20], catecholamine synthesis by the adrenal gland [21], and others [22], and it remains unclear if these phenotypes have been altered by selection on *Epas1*, particularly in other highland taxa. A more detailed understanding of the phenotypic effects of HIF variation is needed in order to ascertain the general role of regulatory pleiotropy in multi-trait physiological adaptation to high altitude.

We used the North American deer mouse (*Peromyscus maniculatus*) to examine links between genetic variation in HIFs and multiple physiological adaptations to high altitude. Within the continental U.S., deer mice are distributed across an altitudinal range of ~4500 m, and have consequently emerged as a prominent model for studies of the mechanisms of adaptation [23–31]. Deer mice native to the Rocky Mountain highlands have evolved a unique physiology that includes suites of adaptations linked to known phenotypes related to HIF signaling (e.g. hematological function, heart rate, tissue capillarity, and metabolic fuel use) [25,26,31–39]. Given the evidence for multi-trait physiological adaptation to high altitude in deer mice, and the recent indications that *Epas1* has been a repeated target of natural selection in multiple highland specialists, we hypothesized that adaptive phenotypic variation is attributable, at least in part, to naturally segregating genetic variation in genes that encode HIFs.

Results

Epas1 genotype varies with altitude in deer mice

In order to examine altitudinal patterns of allele frequency variation of the genes encoding HIFs, and to put these patterns into a broader genomic context, we sequenced the exomes of 37 lowland mice from Lincoln, NE (430 m a.s.l.), and 48 highland mice from Mt. Evans, CO (4350 m a.s.l.). Fifteen mice from a lowland population in Merced County, CA (~320 m a.s.l.), were included to infer polarity of DNA changes in highland mice. All exomes were sequenced using a custom Nimblegen probe set targeting exons from 25,246 nuclear genes (see [Materials and Methods](#)). Captured exomes were paired-end sequenced on an Illumina HiSeq 4000 and mapped to a reference genome (NCBI GCA_000500345.1 Pman_1.0). The final set of quality-filtered sites consisted of 5,182,530 high-quality bi-allelic variants sequenced at approximately 18X coverage (S1 Fig). Analyses of population genetic structure (using PCA [40] and Admixture [41]), revealed that all three populations were genetically distinguishable (S2 Fig and S3 Fig). Pairwise F_{ST} values (estimated with Weir's Theta [42]) between Mt. Evans and Lincoln were $0.025 \pm 3.16e-5$ (mean \pm SEM), between Mt. Evans and Merced were $0.025 \pm 6.54e-5$, and between Lincoln and Merced were $0.044 \pm 8.00e-5$.

Based on these results, we calculated the population branch statistic (PBS [13]) for each single nucleotide polymorphism (SNP) to identify variants that exhibit extreme allele frequency changes in the highland population (Mt. Evans) relative to both lowland populations (Lincoln and Merced) (S4 Fig). Among the upper 0.1% of the PBS distribution, the only SNPs located in HIF genes were three SNPs located in the HIF-2 α gene *Epas1* (Fig 1A, S5 Fig); one of these SNPs was located in the 3'UTR, one was a non-synonymous polymorphism located at site 755

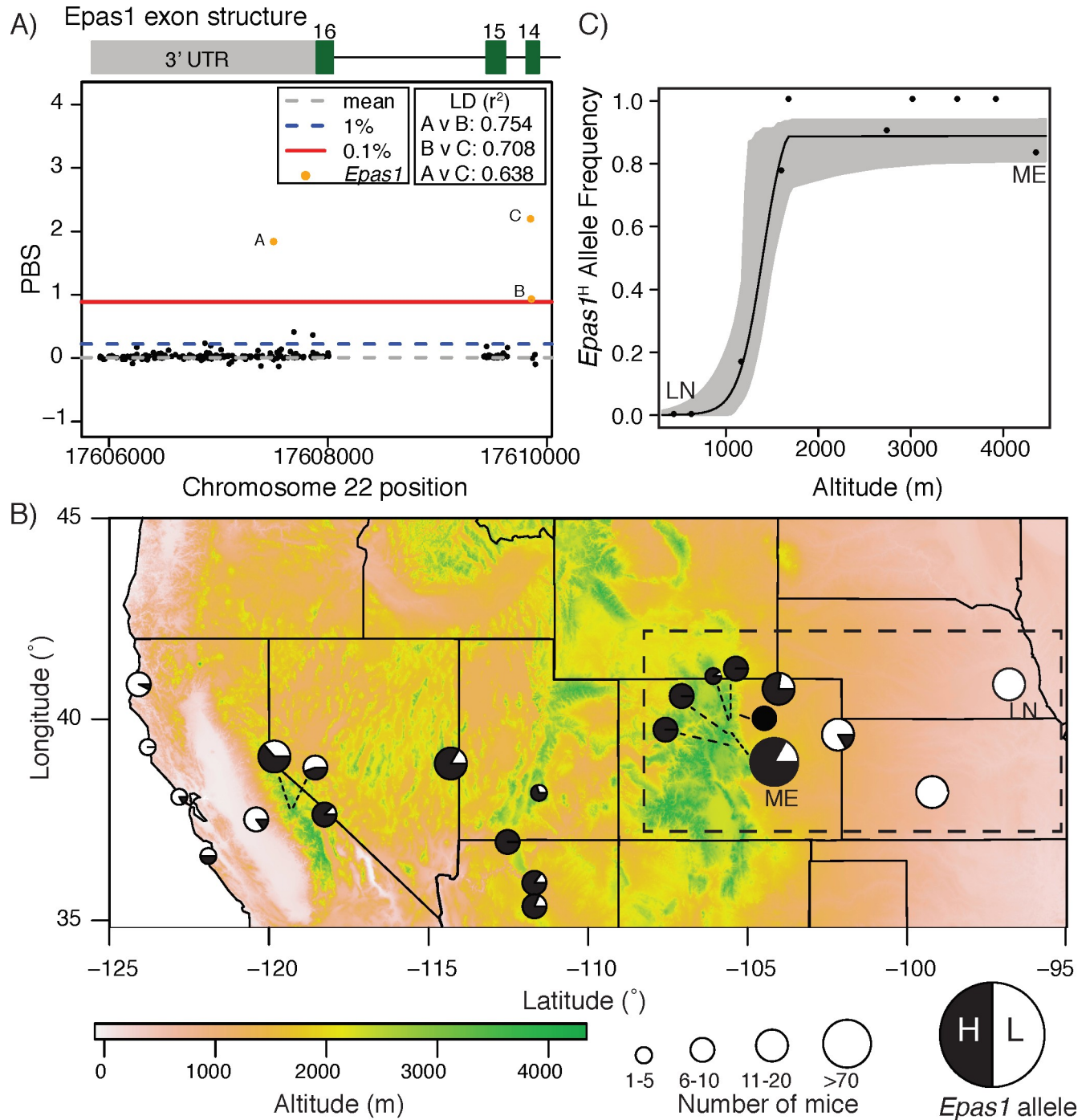


Fig 1. *Epas1* is an exome-wide outlier under spatially varying selection in *P. maniculatus* along altitudinal gradients. A) Manhattan plot of PBS values for all SNPs (black dots) located within the last three exons of *Epas1* (exon numbers provided above schematic). Exome-wide values for mean, top 1%, and top 0.1% percentile PBS values are shown, and three outlier SNPs in *Epas1* are highlighted in orange (see key). Pairwise linkage disequilibrium estimates (measured with the squared correlation coefficient, r^2) for each SNP pair are provided. B) Geographic variation in ^{Thr755Met} *Epas1* allele frequency for 23 populations in the Rocky Mountains and Great Plains, USA. Pie charts are shaded according to frequency of high-altitude or low-altitude allele, with size indicating number of mice sampled (see key). C) Clinal variation in ^{Thr755Met} *Epas1* allele frequency for 10 *P. maniculatus* populations sampled along a 4500 m altitudinal cline from the Great Plains of Nebraska to the Rocky Mountains in Colorado. In (B) and (C), Mt. Evans (ME) and Lincoln (LN) populations are labeled. Dashed box in (B) shows populations chosen for assessing clinal variation in (C). See S1 Table for details on sampling location and *Epas1* allele frequencies.

<https://doi.org/10.1371/journal.pgen.1008420.g001>

in the 14th exon that changed threonine to methionine (^{Thr755^{Met}}), and one was a synonymous polymorphism also located in the 14th exon. The highest-ranking SNP of these three was the non-synonymous, polarity-altering ^{Thr755^{Met}} polymorphism (PBS upper 0.1%; Fig 1A). Due to significant linkage disequilibrium between alleles at the three closely linked *Epas1* SNPs (Fig 1A), and because there were no SNPs in any of the genes that encode HIF-1 α or HIF-3 α in the upper 0.1% of the empirical PBS distribution, we focused our subsequent analyses on the ^{Thr755^{Met}} mutation in *Epas1*.

To more broadly assess the relationship between *Epas1*^{Thr755^{Met}} and elevation, we genotyped an additional 266 deer mice collected from 23 sites across the western U.S. (S1 Table). We found that the Met-755 allele (henceforth called the *Epas1*^H allele) is significantly and positively correlated with altitude ($r^2 = 0.589$, $p < 0.001$; Fig 1B; S6 Fig). For a single altitudinal transect connecting Lincoln to Mt. Evans, variation in *Epas1* allele frequency is best explained as a sigmoidal cline centered at 1399.5 m a.s.l. (95% CI 1192.99–1493.01 m a.s.l.) (Fig 1C). Notably, the *Epas1* cline is similar in shape, width, and center to that of β -globin [43] (S7 Fig), a locus known to be under selection in high-altitude deer mice [28,43,44]. To infer character polarity of the amino acid change, we genotyped mice from nine additional *Peromyscus* species, including *P. keeni*, *P. melanotis*, *P. hylocytes*, *P. attwateri*, *P. melanophrys*, *P. eremicus*, *P. polionotus*, *P. leucopus*, as well as an outgroup rodent species, *Reithrodontomys montanus*. This broader phylogenetic sampling suggests that the high-altitude variant, *Epas1*^H, is the derived allele within the *P. maniculatus* subclade (S2 Table; SI Results).

***Epas1* genotype is associated with physiological traits that influence oxygen homeostasis**

We tested for physiological effects of allelic variation at *Epas1* using deer mice captured on the summit of Mt. Evans. *Epas1*^H and *Epas1*^L alleles segregate in this population, occurring at frequencies of 0.83 and 0.17, respectively (Fig 1), which allowed us to isolate the effects of genotype on an otherwise randomized genomic background. We developed a restriction digest protocol to genotype mice in the field (see Methods), and then subjected mice of known genotype to a series of tests to characterize variation in traits that influence O₂ homeostasis under hypoxia. We used whole-body plethysmography and pulse oximetry during a step-wise hypoxia exposure [20 min at 21 (sea-level), 12 (equivalent to Mt. Evans altitude), 10, 8, and 6 kPa] to test for genotypic effects on acute respiratory and cardiovascular responses to hypoxia: breathing frequency and tidal volume, rate of O₂ consumption (VO₂), arterial O₂ saturation, and heart rate. Forty-eight hours following plethysmography and pulse oximetry, mice were exposed to deep hypoxia (6 kPa) for 2 hours and then euthanized. This duration of exposure to 6 kPa O₂ was chosen in order to strongly stimulate the HIF-induced transcriptional response, as supported by previous observations that this hypoxic treatment strongly induces the expression of *Vegfa*, a key HIF target, in many organisms [44]. Blood, heart, adrenal glands, lungs, and gastrocnemius muscle were sampled for transcriptomic profiling and/or for morphological and histological analysis.

We did not detect significant effects of allelic variation at *Epas1* on some traits that are indicative of chronic exposure to hypoxia or that otherwise influence O₂ transport and utilization. Unlike in studies of indigenous Tibetans [12], *Epas1* genotype did not affect hematocrit or hemoglobin concentration at high altitude (S3 Table, S4 Table). Similarly, we did not detect any genotypic differences in the fiber size (S8 Fig, S9 Fig) or the activities of oxidative enzymes in the gastrocnemius muscle (S5 Table, S10 Fig). There were trends toward reduced muscle capillarity in individuals that were homozygous for the lowland allele (*Epas1*^{L/L}), and reduced lactate dehydrogenase activity in the muscle of individuals that were homozygous for the

highland allele (*Epas1*^{H/H}), but these differences were not statistically significant when compared to all other genotypes (S8 Fig, S9 Fig, S10 Fig).

With respect to respiratory and cardiovascular function under acute hypoxia, we also did not detect any genotypic differences in breathing (total ventilation, breathing frequency, tidal volume), VO₂, body temperature depression, or pulmonary O₂ extraction (S11 Fig, S12 Fig, S6 Table). However, *Epas1* genotype did affect heart rate under ecologically relevant levels of hypoxia: resting heart rates in normoxia (21 kPa O₂) were similar across genotypes, but individuals that were homozygous for the highland allele (*Epas1*^{H/H}) maintained higher resting heart rates during hypoxia exposure compared to the other two genotypes (*Epas1*^{L/L}) (Fig 2). We detected a significant main effect of genotype on heart rate ($F_{2,148} = 3.8$; $p = 0.03$), but a non-significant interaction ($p > 0.05$), suggesting that *Epas1*^{H/H} mice generally maintained higher resting heart rates. The genotypic difference in heart rate was most pronounced at 12 kPa O₂, which approximates PO₂ at the summit of Mt. Evans (Fig 2). However, the magnitude of the increase in heart rate from normoxia to 12 kPa O₂ was greatest in *Epas1*^{H/H} mice (S13 Fig), suggesting that *Epas1* genotype may have influenced the heart rate response to hypoxia at the environmental PO₂ that are realistic at the high-altitude field site. Heart rate did not differ between heterozygotes and homozygotes for the lowland allele at any PO₂ (Fig 2). We observed a steady decline in resting heart rate for all three genotypes as the level of hypoxia increased at PO₂ below 10 kPa (main effect of PO₂: $F_{4,148} = 19.741$, $P < 0.001$), likely as a consequence of the depression in VO₂ and body temperature under extreme hypoxia (S12 Fig).

***Epas1* genotype affects the regulation of HIF target and catecholamine genes**

We used an RNA-seq approach (TagSeq [45]) to test whether *Epas1* genotypes differ in gene regulation in two tissues affecting heart rate under hypoxia: the adrenal gland (which affects heart rate and vasoconstrictive responses by secreting catecholamines) and the left ventricle of the heart. For each tissue we measured transcriptome-wide patterns of gene expression, and the expression of two candidate gene sets: HIF target genes and genes involved in catecholamine biosynthesis, secretion, and signaling (S7 Table). Full results of candidate gene differential expression analysis are available in the online supplement (S8 Table). Overall, this analysis revealed a significant association between *Epas1* genotype and the regulation of genes in HIF- and catecholamine-related pathways in both tissues.

In the adrenal gland, we detected a subtle but significant shift toward reduced expression of candidate genes in mice possessing the high-altitude *Epas1* allele (Fig 3A and 3B). Kolmogorov-Smirnov (K-S) tests revealed significant differences in the distribution of log fold-change values for each comparison of *Epas1*^{L/L} vs. *Epas1*^{H/L} and *Epas1*^{H/H} in catecholamine-associated genes (Fig 3A and 3B), but not HIF targets ($p > 0.05$). Specifically, log-fold change values were significantly more negative for candidate genes in *Epas1*^{H/L} mice compared to the transcriptome-wide background (Fig 3A and 3B), indicating a reduced expression of these genes in mice that carry *Epas1*^H alleles. To test the robustness of this result, we generated a null distribution of K-S test D-statistics by drawing 1000 random gene sets that were equal in size to the candidate catecholamine gene set ($n = 79$). This randomization procedure demonstrates that the D-statistics calculated for both genotypic comparisons were above the 99% quantile of the null distribution (Fig 3B inset). The pattern of down-regulation of catecholamine-related genes is consistent with recent findings that, compared to low-altitude deer mice from Nebraska, high-altitude mice express lower levels of DOPA decarboxylase in the adrenal medulla and exhibit reductions in catecholamine release from adrenal chromaffin cells [46]. Moreover, HIF-2 α has been shown to be a positive regulator of catecholamine synthesis in

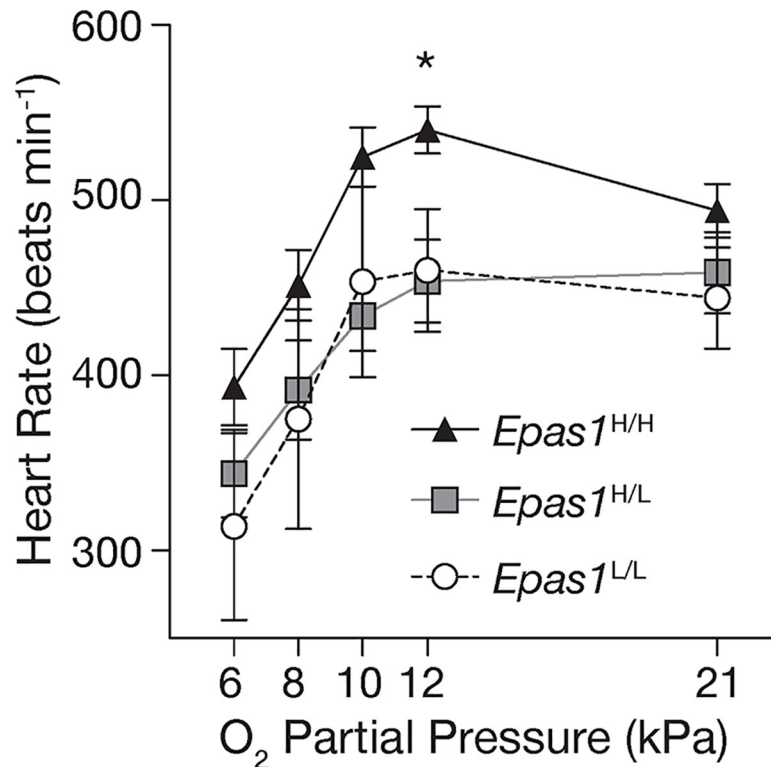


Fig 2. Deer mice that were homozygous for the highland *Epas1* variant exhibited higher heart rates when exposed to environmentally realistic levels of hypoxia at 4300 m altitude (12 kPa O₂). Measurements were made using a MouseOx Plus collar. * Significant main effect of *Epas1* genotype in a mixed linear model. n = 26 *Epas1*^{H/H}, n = 13 *Epas1*^{H/L}, and n = 4 *Epas1*^{L/L} variants.

<https://doi.org/10.1371/journal.pgen.1008420.g002>

adrenal chromaffin cells of rats [21], suggesting that the high-altitude *Epas1* variant leads to a direct reduction in gene expression of enzymes involved in catecholamine biosynthesis, and thereby reduces circulating catecholamine levels.

In a related analysis, we found that positive regulators of catecholamine processes ($n = 15$) were downregulated in mice possessing the high-altitude allele (mean log fold-change between *Epas1*^{H/H} and *Epas1*^{L/L}: -0.04 ± 0.17), relative to genes known to be negative regulators of catecholamines ($n = 13$; mean log fold-change = 0.23 ± 0.19). This trend, though not statistically significant ($p > 0.05$) is consistent with the hypothesis that possessing the high-altitude *Epas1* allele is associated with a downregulation of genes that positively influence catecholamine processes. Due to the small size of the subset of genes for which a directional influence could be established, and the lack of statistical significance, these results should be viewed with caution.

In contrast to the adrenal gland, candidate gene expression in the left ventricle was significantly higher in mice possessing *Epas1*^H alleles, but this effect was subtle and only significant for HIF target genes (Fig 3C and 3D). K-S tests revealed a significant shift toward more positive distribution of log fold-change values in *Epas1*^{H/H} (Fig 3C) and *Epas1*^{H/L} (Fig 3D) mice. Randomization procedures indicated that the empirical D-statistic falls outside of the 99% quantile of the null distribution for both comparisons (Fig 3D). We note that several genes in the top 10% of the distribution of log fold-change in expression (adrenomedullin [*Adm*], endothelin [*Edn1*], and atrial natriuretic peptide [*Nppa*]; S8 Table) are known effectors of vasodilation [47–49], suggesting that improved O₂ supply to cardiac tissue may be positively influenced by *Epas1* genotype.

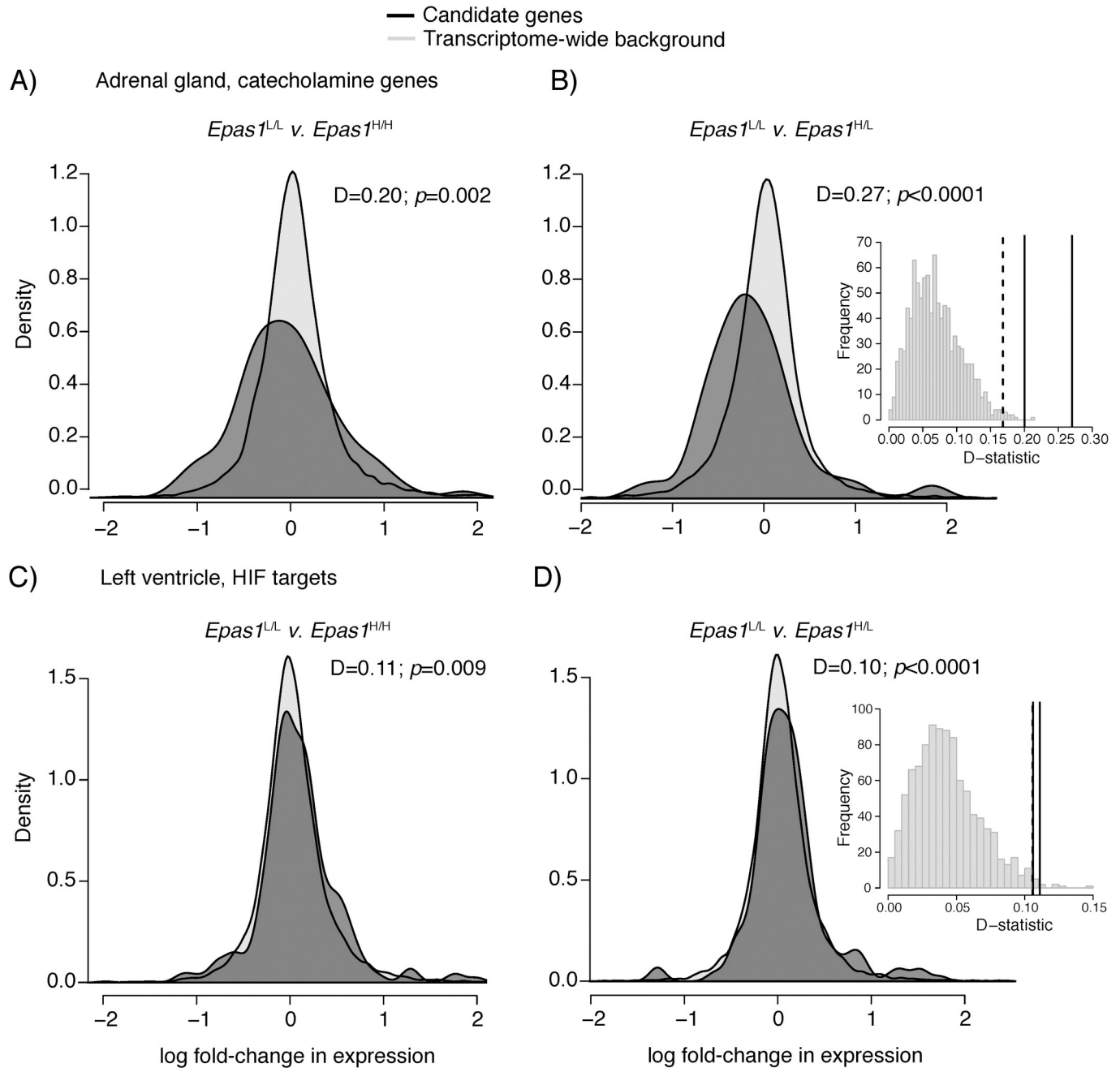


Fig 3. *Epas1* genotype affects the regulation of HIF and catecholamine genes. Distribution of log fold-change values between *Epas1^{LL} v. Epas1^{HH}* and *Epas1^{HL}* for candidate genes (black) compared the the background transcriptome-wide distribution (grey) for adrenal catecholamine genes (A-B) and left ventricle HIF targets (C-D). Insets show the distribution of K-S test D-statistics for 1,000 randomly permuted datasets tested against the transcriptome-wide background. Dashed indicated the 99% quantile of the null distribution, while solid lines indicate the observed D-statistic for each comparison.

<https://doi.org/10.1371/journal.pgen.1008420.g003>

Importantly, none of the genes in these pathways were differentially expressed among genotypes after correcting for multiple testing in either tissue (FDR >0.05), nor were any other genes in either transcriptome. This result suggests that effects of *Epas1* genotype on the regulation of any single gene are weak in these tissues. We note that the O₂ pressure (6 kPa) used to stimulate gene expression was strong, and led to uniform metabolic depression across

genotypes (Fig 2) potentially masking genotypic differences in expression that may exist at less extreme levels of hypoxia. Future research will examine whether 12 kPa O₂, the level leading to the largest genotypic differences in heart rate (Fig 2), elicits greater genotypic difference in the expression of HIF and catecholamine target genes, or potentially other unknown pathways. Nevertheless, our results demonstrate that the combined effects of multiple subtle, but concerted, shifts in expression of HIF target genes and genes in catecholamine-related pathways were detectable among genotypes.

Hypoxia-related genes, including *Epas1*, are targets of positive selection in highland deer mice

To formally test for a history of spatially varying selection on *Epas1* polymorphisms, we performed a demographically-corrected selection scan. We first estimated effective population sizes (N_e), divergence times (T), and pairwise migration rates (m) for two pairs of populations (Mt. Evans-Lincoln and Mt. Evans-Merced) by modeling the folded two-dimensional site frequency spectra (2D-SFS) derived from variation at synonymous SNPs using $\partial a \partial i$ [50]. The best-fitting demographic model (S14 Fig) allowed for variation in gene flow among loci by including two symmetrical migration rate parameters applied to proportions P and $1-P$ of loci, following [51], which produced significantly better fit to the data ($p = 0$; adjusted likelihood ratio test using the Godambe Information Matrix [52]). For Mt. Evans and Merced, we estimated that approximately 84.2% of SNPs experience a relatively high migration rate (2.07 migrants/generation), while the remaining SNPs experience a substantially lower migration rate (0.08 migrants/generations). Similarly, between Mt. Evans and Lincoln, we estimate that approximately 86.4% of SNPs experience a migration rate of ~ 1.75 migrants/generation while remaining SNPs have a rate of ~ 0.08 migrants/generation. Under these models, we estimated effective population sizes of approximately 368,000 (95% CI: 266,977–470,061) for Mt. Evans, 220,000 (95% CI: 170,878–270,767) for Lincoln, and 371,000 (95% CI: 266,871–477,310) for Merced populations (S9 Table). The inferred split time between Mt. Evans and Lincoln populations was approximately 217,000 generations ago (95% CI: 180,998–254,122 generations ago) and the inferred split between Mt. Evans and Merced was 190,000 generations ago (95% CI: 127,569–253,390 generations ago) (S9 Table).

We established a null PBS distribution by simulating 500,000 neutral SNPs (85% with the high migration rates and 15% with the low migration rates) across Mt. Evans, Merced, and Lincoln populations in *msms* [53] under our estimated demographic model, assuming no direct gene flow between Merced and Lincoln (S15A Fig). This approach results in a conservative null model for selection because SNPs simulated under low migration rates between populations likely mimic SNPs that experience local selection. After calculating PBS values [13] from these simulated SNPs, we used the distribution to identify outliers above the simulated 99.9th percentile (corresponding PBS: 0.252). There were 37,169 SNPs located in 6,913 genes above the 99.9th percentile of the simulated distribution (red dashed line in S15 Fig). The Thr⁷⁵⁵Met *Epas1* SNP was highly significant (S15B Fig), as were the two linked noncoding SNPs (S15B Fig). These results provide strong evidence for spatially-varying selection on *Epas1* genotype and suggest that the associated phenotypic effects have fitness consequences in the wild.

Although we had a specific focus on the role of *Epas1* in physiological adaptation to high altitude, our demographically-corrected exome scan also identified a number of other promising candidates for high-altitude adaptation. Among the PBS outliers relative to the simulated null, 37 GO categories and 13 KEGG pathways were significantly enriched (FDR p -value < 0.05 ; S10 Table). Many of these enriched categories are related to known physiological

mechanisms for maintaining homeostasis under hypoxia, such as “response to oxygen-containing compound” (GO:1901700), “regulation of systemic arterial blood pressure” (GO:0003073), and “circulatory system process” (GO:0003013). We focused our examination on outlier SNPs that are located within 1,247 hypoxia-related genes identified by Zhang *et al.* [14] (S11 Table) that represent a set of candidates compiled from “hypoxia” and “hypoxia inducible factor” keyword searches in multiple sources [14]. Of the 6,913 genes with outlier SNPs, 353 genes overlapped with the set of 1,247 hypoxia-related genes from Zhang *et al.* [14] (S11 Table; S12 Table; Fig 4), representing a significant enrichment of hypoxia-related genes (one-sided Fisher’s exact test; FDR-corrected p -value <0.001). *Epas1* was the tenth highest ranking gene (S12 Table).

The top three hypoxia-related genes were *Collagen type I alpha 2 (Col1a2)* (highest-ranking SNP (PBS: 3.33), *Integrin subunit alpha 7 (Itga7)* (PBS: 3.18) and *Potassium calcium-activated channel subfamily M alpha 1 (Kcnma1)* (PBS: 2.82). *Col1a2* encodes one of the most abundant types of collagens that is a ubiquitous component of connective tissue in several organs, whereas *Itga7* and *Kcnma1* may both play roles in muscle structure and function. *Itga7* is expressed in skeletal and cardiac muscles, where it may play a developmental role [54], and *Kcnma1* encodes the pore-forming subunit of an ion channel that is integral to smooth muscle control [55]. Other high-ranking genes of note include *Ceruloplasmin (Cp)*, which was the seventh highest ranking gene (PBS: 2.55; S12 Table) and is involved in iron transport across the cell membrane, in stimulation of erythropoiesis, and in nuclear translocation of HIF1 [56]. Further exploration of these hypoxia-related genes, as well as other targets of selection in high-altitude deer mice, is the focus of an ongoing study.

Discussion

While many studies have identified hypoxia-inducible factors (HIFs) as candidates for high-altitude adaptation (e.g., [8,13–15,57,58]), few have experimentally documented phenotypic effects of mutations in these genes on aspects of systems-level physiology [18]. Yet, these types of genotype-to-phenotype association studies are necessary for identifying functional links that can advance multiple fields from evolutionary biology to biomedicine [59,60]. We combined a series of complimentary population genetic analyses and physiological experiments to test the role of HIFs in high-altitude adaptation of deer mice. We first identified a non-synonymous and polarity-altering polymorphism in the coding region of *Epas1* (which encodes HIF2 α) that exhibited an extreme allele frequency difference between highland and lowland populations (Fig 1A). Moreover, the high-altitude *Epas1*^H allele, which is derived in the *P. maniculatus* sub-clade, varied predictably with altitude in mice sampled throughout the western United States (Fig 1B and 1C). These results suggested that variation at *Epas1* may contribute to well-characterized physiological differences observed between highland and lowland deer mice [25,26,31–39]. Physiological tests of this hypothesis demonstrated that *Epas1* polymorphism was not associated with many traits known to be regulated by HIFs [11]. Most notably we did not detect an association between *Epas1* genotype and hematocrit or hemoglobin concentration (S3 Table, S4 Table) unlike studies in high-altitude indigenous Tibetans [12], nor did we detect associations with adaptive variation in breathing pattern [34] or skeletal muscle fiber type [32] shown in high-altitude deer mice (see S5 and S6 Tables). If the observed mutation at *Epas1* does affect such traits, our results suggest that other mechanisms compensate for these effects in mice that have developed at high altitude.

Although we did not detect an effect of *Epas1* genetic variation on several HIF-related traits, we documented an unprecedented relationship between *Epas1* genotype and cardiovascular function. Experimental hypoxia exposures demonstrated that mice homozygous for *Epas1*^H

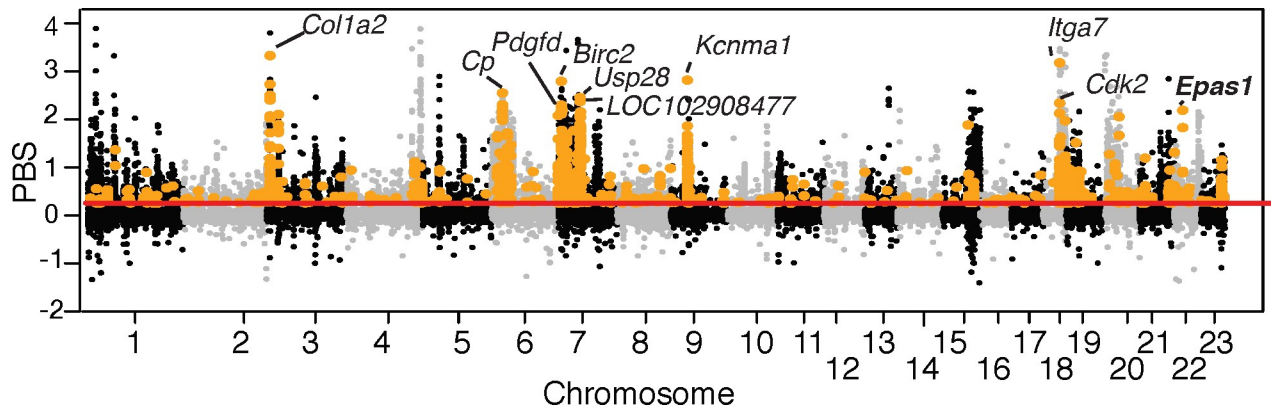


Fig 4. *Epas1* is an outlier in a demographically-controlled selection scan. Exome-wide distribution of population branch statistic (PBS) for Mt. Evans mice based on 5,182,530 SNPs from the exome. Horizontal line (red) indicates the top 0.1% percentile PBS of 500,000 neutral SNPs simulated under a realistic demographic scenario, and SNPs in hypoxia-related genes are highlighted in orange. The top ten hypoxia-related genes are labeled, with *Epas1* indicated in bold text. SNPs with a PBS value below the top 0.1% percentile have been randomly down-sampled (1:20) for ease of plotting.

<https://doi.org/10.1371/journal.pgen.1008420.g004>

maintain an elevated heart rate under physiologically and ecologically relevant levels of hypoxia (Fig 2). Moreover, *Epas1* genotype appears to have systematic effects on pathway gene expression, leading to downregulation of genes involved in catecholamine biosynthesis and secretion in the adrenal gland (Fig 3A and 3B), and upregulation of HIF targets in the left ventricle of the heart (Fig 3B and 3C). While the effects of *Epas1* genotype on the expression of any single gene are weak, the combined effects of subtle but concerted shifts in expression of genes in these candidate pathways were detectable and varied predictably among genotypes. Finally, formal demographically-controlled selection scans revealed that *Epas1*, and a number of other genes in hypoxia response pathways, have been a target of natural selection at high altitude (Fig 4). These results suggest that the associated phenotypic differences in cardiovascular function and gene regulation contribute to fitness differences in the wild.

This study provides the first documentation of a relationship between naturally occurring genetic variation at *Epas1* and heart rate under hypoxia. The maintenance of an elevated heart rate during hypoxia could be the direct phenotypic target of selection on *Epas1* in order to improve circulatory O₂ delivery at high altitude. Assuming that there are not opposing differences in stroke volume between genotypes, increased heart rate should result in an increased cardiac output and thus enhanced O₂ delivery to systemic tissues [10]. Indeed, mice that were homozygous for the highland *Epas1* genotype tended to have slightly larger ventricles (Table S4), which although not statistically significant, suggest that lower heart rates are not compensated for with increases in heart size (and potentially associated increases in stroke volume). Elevated heart rates during hypoxia could also be a secondary consequence of adaptive changes in other functions of the cardiovascular control system that are the direct targets of selection. One possible target of selection is catecholamine release from the adrenal medulla, which we have recently shown is attenuated in high-altitude deer mice [46]. The genetic basis for this attenuation is unknown, but the patterns of variation in expression for genes related to catecholamine synthesis and release suggest that genetic variation in *Epas1* may be involved. Catecholamine release in hypoxia normally acts to induce vasoconstriction and constrain blood flow to many peripheral tissues [61], so the attenuation of catecholamine release in highland mice may serve primarily to minimize this effect and improve tissue blood flow during hypoxia. However, hypoxic vasoconstriction could normally lead to feedback activation of the baroreflex, which would tend to reduce heart rate and oppose other factors that tend to stimulate heart rate in hypoxia (i.e., activation of sympathetic neurons innervating the heart). This

potential secondary effect of hypoxic vasoconstriction would be minimized by an attenuation of adrenal catecholamine release, such that heart rate would rise more in response to hypoxia. Therefore, in this hypothetical example, the primary target of selection (improvement in regional tissue blood flows via reductions in catecholamine release) has secondary consequences on the heart rate response to hypoxia.

Whatever the mechanism, the observed effects of *Epas1* genotype within highland mice mirror genetically-based population differences in heart rate between highlanders and lowlanders [34], suggesting that evolved population differences may result from allelic variation at *Epas1*. Humans native to the Qinghai-Tibetan plateau (2200–5200 m a.s.l) reach higher maximal cardiac outputs during exercise compared to closely related lowland Han Chinese when tested at high altitude [62]. These results suggest that changes in cardiovascular function or control—either at rest, as in deer mice, or during exercise, as in Tibetan humans—may be a common adaptation to high altitude. The potential benefit to circulatory O₂ delivery conferred by these cardiovascular changes is likely one of many adaptations that improve metabolic homeostasis across systemic tissues in highlanders. These other potential adaptations include evolved changes in breathing and respiratory gas exchange [34], higher hemoglobin O₂ affinity [28], enhanced capacity for O₂ diffusion into metabolically active muscles [26,32,37], as well as changes in the density, intracellular distribution, and function of muscle mitochondria [37,38]. All of these modifications are likely to contribute to an enhancement of aerobic performance under O₂ deprivation [24,25,32].

The results of this study demonstrate a role for coding changes in a transcription factor in environmental adaptation. The majority of the systems-level traits we measured (e.g., breathing, metabolism) were remarkably similar between *Epas1* genotypes, as were the transcriptome-wide effects of *Epas1* genotype on gene expression in the adrenal gland and heart, suggesting that the *Epas1* amino acid mutation has highly targeted phenotypic effects. Our results suggest that selection on high-level transcription factors such as *Epas1* contribute to local adaptation, so any negative pleiotropic effects associated with the evolved changes must be compensated by other mechanisms.

Materials and methods

Ethics statement

We handled and sampled mice in accordance with the University of Montana's Institutional Animal Care and Use Committee (AUP 029–16), the Colorado Department of Fish and Wildlife (License Number: 17TR2168a) and the United States Forest Service (Authorization ID: CLC772). Following protocol, mice were euthanized with an isoflurane overdose followed by decapitation.

Exome design, capture, and high-throughput sequencing

To identify all annotated exons, we downloaded the *Peromyscus maniculatus bairdii* GFF v101 from NCBI (Accession GCF_000500354.1), and extracted all features annotated as an exon. The final set of unique, non-pseudogenized exonic regions consisted of 218,065 exons in 25,246 genes. A custom Roche NimbleGen SeqCap EZ Library kit capture a total of 226,973 regions (77,559,614 bp).

We extracted DNA from tissues of 85 deer mice (Lincoln, NE: n = 37; Mount Evans, CO: n = 48) and sheared DNA to ~300 bp using a Covaris E220 Focused Ultrasonicator. Genomic libraries for each individual were prepared using 200 ng of sheared DNA with a NEBNext UltraII kit and unique index following manufacturer's protocols. We pooled batches of 24 indexed libraries prior to target enrichment and PCR amplification following the NimbleGen

Seq Cap EZ protocol (Roche). Quality control for each capture pool included a check of size distribution and a check for enrichment of targeted regions and no enrichment of non-targeted regions using qPCR. Each capture pool of 24 individuals was sequenced with 100 bp paired-end sequencing on an Illumina HiSeq 4000. We extracted and quantified DNA samples for the California deer mice (Merced, CA; $n = 15$) at the Museum of Vertebrate Zoology, UC Berkeley, before shearing one μg of genomic DNA to less than 500 bp with a Biorupter (Diagenode). We prepared barcoded Illumina sequencing libraries using the Meyer and Kircher [63] protocol, then amplified libraries with Phusion High-Fidelity DNA Polymerase (Thermo Scientific) for 6–8 cycles during the indexing PCR. Exome enrichment was conducted with a custom capture design from the SeqCap EZ Developer Library (Nimblegen) that was almost identical to that used in the 85 non-CA samples. Captures were quantified, pooled proportionally to the amount of DNA in each, and sequenced using 100bp pair-end sequencing on an Illumina HiSeq4000.

Data pre-processing and variant discovery on all samples followed the recommendations of the Broad Institute GATK v3.7-0-gcfedb67 Best Practices pipeline. We trimmed reads of adapter sequences and for a minimum base quality of 20 using *fastq_illumina_filter 0.1* (<https://mcbl.readthedocs.io/en/latest/mcbl-tutorials-PF-clean.html>) and *trim_galore 0.3.1* (http://www.bioinformatics.babraham.ac.uk/projects/trim_galore/). We used *bwa mem* [64] to align and map forward and reverse reads to the *Peromyscus maniculatus baiardii* genome. We removed duplicates using *samtools rmdup* [65], then added read group information using *picard*. (<http://picard.sourceforge.net>). To generate a set of “known” variant sites for GATK Base Quality Score Recalibration (BQSR), we genotyped each individual using *samtools mpileup* (-q 30 -Q 30) and *bcftools call*, then filtered genotypes to have a minimum depth of coverage (minDP) of 10 and minimum genotype quality (minGQ) of 30, and only used those variants observed in at least two individuals. The resulting set of variant positions was used with the -knownSites flag during GATK BQSR. A subsequent round of BQSR was completed and convergence of quality scores was verified using GATK *AnalyzeCovariates*. To genotype each sample, we used GATK *HaplotypeCaller* with the ‘--emitRefConfidence’ flag, then called variants GATK *GenotypeGVCFs*. We combined GVCFs and filtered them to remove SNPs with a quality of depth < 2.0, a FS > 60, mapping quality < 40, mapping quality rank sum < -12.5, and read position rank sum < -8.0. We implemented all processing steps in GATK using the ‘--interval’ flag, a bed file of capture regions, and a ‘--interval_padding’ of 200 bp. These processing steps resulted in a total of 106,883,914 sites among all individuals.

After assessing the quality of filtered reads using the *vcftools* package [66], we further filtered variants so that a site was called in at least 50% of individuals, was bi-allelic, and each site had a minDP of 5 and minGQ of 20. We proceeded with a set of 5,183,434 high-quality bi-allelic variants, with a mean depth of coverage of $18.10 \pm 6.38 \times$ (S1 Fig).

Population genetic structure

We assessed population genetic structure of Mount Evans, Lincoln, and Merced mice using principal components analysis within PLINK [40] and Admixture [41]. Prior to running the analyses, we pruned the set of variants to only sites with no missing data, and not linked (using the “--indep-pairwise 50 5 0.5” option within PLINK). The final set of variants for these analyses consisted of 296,196 bi-allelic sites.

Allele frequency variation in HIF genes

In order to examine altitudinal patterns of allele frequency variation of the genes encoding HIF-1 α , HIF-2 α , and HIF-3 α , we calculated pairwise F_{ST} using *vcftools*, then the Population

Branch Statistic (PBS) [13] for each of the 5,183,434 bi-allelic variants. Using the ‘ecdf’ function in R, we used the empirical distribution of PBS values and set a threshold of 99.9% for significance (corresponding PBS: 0.886). We used Ensembl’s Variant Effect Predictor [67] with the *P. maniculatus* reference genome annotation data set to identify SNPs located in HIF genes. For the three outlier SNPs located in *Epas1*, we calculated pairwise linkage between each SNP as the squared correlation coefficient, r^2 , using the ‘--geno-r2’ function within vcfTools [66],

Geographic and phylogenetic survey

To fully assess the geographic and phylogenetic extent of variation in *Epas1*, we genotyped 266 *P. maniculatus* samples from across the western US (S1 Table), plus samples of *P. keeni*, *P. melanotis*, *P. hylocytes*, *P. attwateri*, *P. melanophrys*, *P. eremicus*, *P. polionotus*, *P. leucopus*, *Reithrodontomys montanus*, and *Phyllotis xanthopygus* (S2 Table). We obtained tissue samples from our existing freezer collections or museums (Museum of Southwestern Biology at the University of New Mexico, or Museum of Comparative Zoology, Harvard University). From each sample, we extracted DNA then PCR amplified *Epas1* with custom exonic primers (“epas1_snp_L” and “epas1_snp_R”; S13 Table) designed from the *P. maniculatus bairdii* genome under the following conditions: 94°C for 2 mins; 30 cycles of 94°C for 45 sec, 58°C for 1 min, 72°C for 1 min; then 72°C for 10 mins. To improve amplification specificity for *P. maniculatus* samples, we used modified primers and PCR conditions (“epas1_set1_F” and “epas1_set1_R”; S13 Table): 94°C for 2 mins; 35 cycles of 94°C for 30 sec, 62°C for 30 sec, 68°C for 1 min; then 68°C for 10 mins. Technicians at Genewiz (South Plainfield, NJ) cleaned amplified products and sequenced them in both directions. We called genotypes after aligning sequences to the reference sequence using Geneious 8.1.8. We calculated population allele frequencies within each sampling locality, and obtained elevation for each locality from GPS data recorded upon sampling, or from Google Maps. We mapped these allele frequency data on a map of elevation (data downloaded from www.worldclim.org) using the ‘maps’ package in R. Finally, we placed *Epas1* genotype for each sequenced species on a *Peromyscus* phylogeny constructed previously [68–70].

Cline analysis for *Epas1* and Hemoglobin genes

We tested whether the *Epas1* allele frequencies follow a clinal pattern using the R package HZAR [71]. In HZAR, genetic data are fit to equilibrium cline models using the Metropolis–Hastings Markov chain Monte Carlo (MCMC) algorithm, and parameters such as the cline center (c) and width (w) are estimated. c and w characterize the location within the transect where the variable changes most rapidly, and the values of these parameters can be estimated within HZAR by 15 models that differently estimate the exponential decay on either side of the cline center, as well as the minimum or maximum frequencies. We used as input the *Epas1* allele frequency data and elevation for populations of deer mice sampled across the Rocky Mountain to Great Plains elevational cline, and used a burn-in of 10000. We compared the *Epas1* cline to that for previously published hemoglobin haplotype frequencies in deer mice [43].

Physiological effects of allelic variation at *Epas1*

To test for physiological effects of allelic variation at *Epas1*, we captured deer mice from a single interbreeding population in which the high-altitude allele is segregating. We collected adult deer mice from the summit of Mt. Evans (Clear Creek Co., Colorado, USA; 39° 35′ 18″ N, 105° 38′ 38″ W; 4,350 m above sea level; PO₂ ~ 95.6 mm Hg) in August 2016 and 2017 and screened

the *Epas1* allele (a C/T polymorphism at nucleotide position 2264, hereafter C^{2264T}). From each individual, we sampled an ear clip sample, extracted DNA, then genotyped *Epas1* C^{2264T} using a custom restriction enzyme digest assay. Briefly, we PCR amplified *Epas1* with custom exonic primers (S13 Table) designed from the *P. maniculatus bairdii* genome and amplified under the PCR conditions specified above. For all amplified PCR products, we cut *Epas1* at C^{2264T} by incubating the PCR product with the BsaHI restriction enzyme at 37°C for 1 hour followed by a heat denaturation for 20 mins. We called *Epas1* genotypes via gel electrophoresis (T ~675 bp; C ~300 bp;), then subsequently confirmed field genotypes with Sanger sequencing at Genewiz.

Acute hypoxia responses with pulse oximetry

At the University of Denver Mt. Evans field station (3230 m a.s.l.; ~15kPa O₂), we screened these Mt. Evans mice with alternative *Epas1* genotypes for a suite of physiological responses involved in O₂ transport and utilization and/or known to be influenced by HIFs. We measured hypoxia responses in mice (26 *Epas1*^{H/H}, 13 *Epas1*^{H/L}, and 4 *Epas1*^{L/L}) using previously described barometric plethysmography, respirometry, and pulse oximetry techniques [34,72]. We placed each mouse in a whole-body plethysmograph (chamber volume: 530 ml) that was supplied with hyperoxic air, mixed to simulate the partial pressure of O₂ (PO₂) at sea level (21 kPa O₂, balance N₂), at a rate of 600 ml min⁻¹. We gave mice 20–60 min to adjust to the chamber and stabilize their breathing and metabolism. We recorded measurements for an additional 20 min at 21 kPa O₂, then exposed mice to 20 min stepwise reductions in inspired PO₂ of 12, 10, 8, and 6 kPa. We set the incurrent gas composition by mixing dry compressed gases using precision flow meters and a mass flow controller, such that the desired PO₂ was delivered to the chamber at a constant rate of 600 ml min⁻¹. At the end of the experiment, we measured body temperature (T_b) using a mouse rectal probe. We also measured T_b exactly 24 h later to determine resting T_b (this was used as a proxy for the resting T_b at the start of the experiment, which was not measured to prevent stress to the animal).

We determined breathing and O₂ consumption rate (VO₂) during the last 10 min at each PO₂ by subsampling incurrent and excurrent airflows at 200 ml min⁻¹. For incurrent and excurrent air, we measured water vapor (RH-300, Sable Systems) using a thin-film capacitive water vapor analyzer, then dried air with pre-baked drierite, and measured continuously for O₂ and CO₂ fraction using a galvanic fuel cell O₂ analyzer and infrared CO₂ analyzer (FOX-BOX, Sable Systems). We used these data to calculate VO₂ and CO₂ production rate (VCO₂), expressed at standard temperature and pressure (STP), using appropriate equations for dry air as described by Lighton [73]. We measured breathing frequency and tidal volume from changes in flow across a pneumotachograph in the plethysmograph wall, detected using a differential pressure transducer. We calculated tidal volume using established equations [75,76] and assuming a constant rate of decline in T_b with declining PO₂, which we have previously shown results in similar tidal volumes to those calculated using direct T_b measurements at each PO₂ [72], and is expressed at STP. We calculated the following parameters: total ventilation (the product of breathing frequency and tidal volume), ventilatory equivalent for O₂ (total ventilation divided by VO₂), and percent pulmonary O₂ extraction (VO₂ divided by the product of total ventilation and inspired O₂ fraction). We measured SaO₂ and heart rate using the MouseOx Plus pulse oximeter collar sensors and associated software (Starr Life Sciences, Oakmont, PA, USA). Use of the collars was enabled by removing a small amount of fur from the skin around the neck one day before experiments.

We tested for effects of *Epas1* genotype on cold-induced VO₂ max (thermogenic capacity), an ecologically relevant measure of whole-organism aerobic performance for which there is an

evolved difference between lowland and highland deer mice [24]. To do this we measured maximum rates of oxygen consumption in a hypoxic, heliox atmosphere (21% oxygen, 79% helium) using open-flow respirometry. All trials were conducted at the summit of Mt. Evans. The use of heliox ensures that VO_2 max can be measured without risking cold injury, since rates of heat loss in heliox are several times greater than that of ambient air [74]. For each trial, we equilibrated heliox gas mixtures with atmospheric pressure of the Mt. Evans summit (12 kPa). Mass flow controllers helped pump the heliox mixture into copper coils inside a temperature control chamber. The cooled gas was pumped into an animal chamber and an empty baseline chamber at a rate of $\sim 750 \text{ ml min}^{-1}$. Excurrent air from the animal and baseline chambers was sampled at a rate of $\sim 130 \text{ ml min}^{-1}$, dried with magnesium perchlorate and scrubbed of CO_2 , redried with drierite, and passed through an oxygen analyzer. We defined thermogenic capacity as the maximum VO_2 averaged over a continuous 5-min period. We tested for the influence of genotype on thermogenic capacity using an analysis of covariance (ANCOVA) with body mass as covariate.

Tissue and organ sampling and phenotyping

Mice recovered for 2–3 days after the hypoxia response experiments described above. We exposed recovered mice to 2 hours of deep hypoxia (6 kPa O_2) and euthanized them with an isoflurane overdose followed by decapitation. We collected blood samples for hematocrit (in heparinized capillary tubes, spun for 5 minutes) and hemoglobin content (Hemocue, Sweden). We dissected the heart, then isolated and weighed the ventricles before freezing them separately in liquid N_2 . We determined lung volume by volumetry [75]. We weighed and froze in liquid N_2 one gastrocnemius muscle, then coated the other in embedding medium and froze it in liquid N_2 -cooled isopentane for histology. We froze other organs directly in liquid N_2 .

We measured muscle capillarity using histological methods in a subset of the mice (17 *Epas1*^{H/H}, 13 *Epas1*^{H/L}, and 4 *Epas1*^{L/L}) chosen to ensure a balanced sex distribution (11 *Epas1*^{H/H} males, 6 *Epas1*^{H/H} females, 11 *Epas1*^{L/L} males, 6 *Epas1*^{L/L} females) and body mass ($21.49 \pm 4.05 \text{ g}$ for *Epas1*^{H/H}, $21.76 \pm 5.43 \text{ g}$ for *Epas1*^{H/L}, $21.01 \pm 4.12 \text{ g}$ for *Epas1*^{L/L}; means \pm SEM) between the three groups. We prepared full transverse sections of the gastrocnemius muscle as previously described [32,76]. Briefly, after cutting 10 μm tissue sections transverse to the muscle fiber length using a cryostat, we identified capillaries by staining samples for alkaline phosphatase activity following previous studies [32,76]. We used bright-field microscopy to systematically collect images from across the entire gastrocnemius, and used ImageJ software [77] to count the number of capillaries and muscle fiber in each image and measured capillary density, average number of capillaries per muscle fiber, and average transverse area of muscle fibers. We used NIS-Elements D Imaging Software (v. 4.30, Nikon Instruments) to measure the number, perimeter, and capillary surface densities of individual capillaries within each image. We determined a sufficient number of images to analyze to account for heterogeneity across the gastrocnemius, determined by the number of replicates necessary to yield a stable mean value, following ref. [32]. This required analysis of roughly half of the entire section, with images spread evenly across the section, which was found to be more than sufficient to accurately represent average values across the entire muscle. For all histological measurements, the observer was blind to genotype during analysis.

We used the remaining gastrocnemius muscle tissue in metabolic enzyme assays that we have previously described [76]. After removing embedding medium from the muscle tissues we powdered samples under liquid N_2 and homogenized them in ice-cold homogenization buffer [76]. We centrifuged homogenates at 1000g for 1 min at 4°C, discarded the pellet, and stored the homogenate on ice until assay. We assayed activities of cytochrome c oxidase

(COX), citrate synthase (CS), and lactate dehydrogenase (LDH) in triplicate at 37°C using a 96-well microplate reader. Assay conditions in mM were as follows: COX, 100 KH_2PO_4 , 0.2 reduced cytochrome c^* , pH 8.0; CS, 100 KH_2PO_4 , 0.5 oxaloacetate * , 0.15 acetyl-coA, 0.15 5,5'-dithiobis-2-nitrobenzoic acid (DTNB), pH 8.0; LDH, 100 KH_2PO_4 , 0.15 NADH, 2.5 pyruvate * , pH 7.2. We determined maximal activities by measuring the change in absorbance over time at 550 nm for COX ($\epsilon = 28.5 \text{ mM}^{-1} \text{ cm}^{-1}$), 412 nm for CS ($\epsilon = 14.15 \text{ mM}^{-1} \text{ cm}^{-1}$), and 340 nm for LDH ($\epsilon = 6.22 \text{ mM}^{-1} \text{ cm}^{-1}$), and subtracting the background rate from the rates measured in the presence of all substrates.

Statistical analyses of physiological effects of allelic variation at *Epas1*

To assess the influence of *Epas1* genotype on physiology and tissue/organ phenotypes, we used linear mixed effect models and included body mass, genotype, and acute PO_2 (when appropriate) as fixed effects. We initially included year (2016 or 2017) and sex as random effects, but removed them from all models because they were never found to be significant ($P > 0.25$). We removed body mass from models in which its effect was not significant for variables that we did not have any *a priori* expectation of allometric scaling (heart rate, SaO_2 , hematology, and gastrocnemius muscle capillarity and enzyme activities). We conducted Holm-Sidak pairwise post-tests on significant models, and used R (v. 3.4.3) and the *lme4* package for all statistical analysis, with a significance level of 0.05. We report VO_2 , total ventilation, and tidal volume relative to body mass to enable comparison to the literature, but we used the absolute data (i.e., not expressed relative to body mass) for statistical analyses as described above.

Transcriptomic analysis of differential gene expression

We used high throughput sequencing to test for effects of *Epas1* genotype on gene expression in adrenal gland (8 *Epas1*^{H/H}, 8 *Epas1*^{H/L}, 3 *Epas1*^{L/L}) and heart tissue (7 *Epas1*^{H/H}, 9 *Epas1*^{H/L}, 3 *Epas1*^{L/L}). We chose the adrenal gland because of its role in stimulating heart rate *via* catecholamine release. We assayed gene expression using TagSeq, a 3' tag-based sequencing following ref. [45]. We extracted RNA from 25 mg of tissue using TRI Reagent (Sigma-Aldrich), then assessed RNA quality using TapeStation (Agilent Technologies; $\text{RIN} > 7$). The Genome Sequencing and Analysis Facility at the University of Texas at Austin prepared TagSeq libraries, which were sequenced using Illumina HiSeq 2500. Sequencing generated an average of 4.6M reads per individual. We processed raw reads following Lohman et al. [45] and mapped them to the *P. maniculatus* genome using bwa [64]. We used *featureCounts* [78] to generate a table of transcript abundances. Since genes with low read counts are subject to increased measurement error [79], we excluded those with less than an average of 10 normalized reads per individual using the *filterByExpr* function in *edgeR*. We retained a total of 12,237 and 10,509 genes after filtering for adrenal and heart transcriptomes, respectively.

We used two complementary approaches to compare levels of transcript abundance among *Epas1* genotypes: (1) A whole-transcriptome differential expression analysis was conducted to identify genes that were differentially expressed in each tissue. (2) We performed candidate differential expression analysis on two *a priori* gene sets aimed at testing whether genes related to the HIF cascade and/or catecholamine synthesis/transport exhibited concerted changes in gene expression among alternative genotypes. We conducted the whole-transcriptome differential expression analysis in *edgeR* [80]. The function *calcNormFactors* was used to normalize read counts among all libraries, after model dispersion was estimated for each transcript separately using the function *estimateDisp* [81]. We tested for differences in transcript abundance by first fitting a quasi-likelihood negative binomial generalized linear model to raw count data (*glmQLFit* function), which included a single main effect of genotype (*Epas1*^{L/L} was used as a

reference for comparing against *Epas1*^{H/L} and *Epas1*^{H/H}). P-values were calculated using a quasi-likelihood F test using the *glmQLFTest* function. We controlled for multiple testing by enforcing a genome-wide false discovery rate correction of 0.05 [82]. We identified candidate HIF target genes from the literature [83,84] and Kyoto Encyclopedia of Genes and Genomes database [85] as those with known function in HIF signaling, and those that have an unknown function but contain HIF binding sites [84]. We ascertained catecholamine-related genes based on annotation in the Gene Ontology (GO) database in AmiGO (amigo.geneontology.org). A total of 277 HIF targets and 149 catecholamine related genes (S7 Table) were identified.

To determine whether there were concerted shifts in gene expression for the candidate gene sets among genotypes, we calculated log fold-change in expression between *Epas1*^{L/L} mice and mice heterozygous and homozygous for the high-altitude allele in *edgeR*. The distribution of fold-change values between candidate gene sets and the transcriptome-wide background (candidate genes excluded) was compared using Kolmogorov-Smirnov (K-S) tests using the function *ks.test* in R. We then conducted a randomization procedure to test whether the observed D-statistic for K-S tests was greater than a null distribution; the null distribution of D-statistic values was produced by 1000 random draws of gene sets that were of equal size to candidate sets (adrenal: HIF: $n = 207$; catecholamine: $n = 79$; left ventricle: HIF: $n = 207$; catecholamine: $n = 55$) and comparing those to the transcriptome-wide background.

Demographic modeling and null PBS distribution

We estimated the demographic history of highland and lowland deer mice using synonymous SNPs in *ada2i* [50]. We filtered SNPs in Hardy-Weinberg equilibrium ($p < 0.001$) and excluded sites with $> 25\%$ missing data per population using *vcftools*, resulting in 287,336 SNPs to generate a folded site-frequency spectrum. We then estimated effective population sizes (N_e), divergence times (T), and pairwise migration rates (m) between highland deer mice from Mt. Evans, CO ($n = 48$) and deer mice from Lincoln, NE ($n = 37$) and Merced, CA ($n = 15$). We assumed that any migration between Lincoln and Merced populations would occur indirectly through the central Mt. Evans population and thus we did not perform a pairwise demographic analysis for Lincoln and Merced. For our pairwise population comparisons (Mt. Evans-Lincoln and Mt. Evans-Merced), we calculated maximum-likelihood (ML) parameters for demographic models with and without a single symmetrical migration parameter and with an effective population size parameter (u ; proportional change in N_e relative to the ancestral population immediately following the split). We observed that maximum likelihood parameters under models of no migration or a single symmetrical migration rate strongly underestimated the relative abundance of highly differentiated SNPs, resulting in poor fit to the empirical 2D-SFS (S14 Fig). We also tested a model which included heterogeneous migration rates among loci in the genome. Here, we included two symmetrical migration rates, one for proportion P of SNPs and one for proportion $1-P$ of SNPs, where we also estimate the P parameter. For each demographic model, we performed 25 independent runs with starting parameter values sampled randomly from a uniform prior distribution ($0 < 2N_e m < 10$; $0.01 < 2N_e t < 10$; $0.1 < u < 10$; $0.5 < P < 1.0$). We selected the optimal demographic model based on an adjusted likelihood ratio test using the Godambe Information Matrix [52]. We estimated 95% confidence intervals for population size, divergence time, and migration rate parameters using the Godambe Information Matrix with 100 replicate bootstrap data sets consisting of randomly sampled SNPs spaced at least 10 kb apart (14250 SNPs for each data set). We calibrated theta estimates based on the ratio of all callable sites to SNPs under the same filtering regime and assuming a mutation rate of 5.4×10^{-9} per base per generation (house mouse; ref. [86]).

To establish a null PBS distribution, we simulated 500,000 neutral SNPs across three populations in *msms* [53] under our estimated demographic model. Given our optimal models included two symmetrical migration rate parameters applied to different sets of SNPs we simulated proportion P of SNPs under high migration rates (85%) and proportion $1-P$ of SNPs under low migration rates (15%) and combined the two simulated data sets. We used *msstats* (<https://github.com/molpopgen/msstats>) to obtain F_{ST} values for SNPs between each population and calculated PBS based on the equation in Yi et al. [13].

Demographically corrected exome scan with the Population branch statistic

We used the simulated distribution of PBS values, and set a significance threshold of 99.9% (corresponding PBS_{sim} : 0.199). We focused our examination on outlier SNPs that are located within 1,247 hypoxia-related genes from Zhang *et al.* [14] (S11 Table). The genes from Zhang *et al.* represent a set of candidates compiled from “hypoxia” and “hypoxia inducible factor” keyword searches in multiple sources, including the UCSC Genome Browser, Ensembl, NCBI, UniProt, and RefSeq. For each *P. maniculatus* gene containing outlier SNPs, we found the corresponding *Mus musculus* gene, then used gProfiler [87] to identify enriched gene ontology categories above a false discovery rate corrected significance of 0.05, using strong hierarchical filtering.

Supporting information

S1 Text. File containing supplemental results for population genetic, cline, and physiological analyses.

(DOCX)

S1 Table. Sampling locations and frequency of *Epas1* alleles for 266 *Peromyscus maniculatus* samples used to generate map and cline in Fig 1. Sampling locations in bold text were used to generate cline in Fig 1C.

(XLSX)

S2 Table. Sampling locations, museum accessing numbers, and *Epas1* genotypes for *Peromyscus* and broader phylogenetic sampling.

(XLSX)

S3 Table. Blood characteristics and organ masses of *Epas1* variants of deer mice. Values are expressed as mean \pm SEM; $n = 31$ for *Epas1*^{H/H}, $n = 13$ for *Epas1*^{H/L}, $n = 4$ for *Epas1*^{L/L} variants.

(XLSX)

S4 Table. F- and P-values for mixed linear effect models of blood and organ mass variables in *Epas1* variants of deer mice. n.s. not significant and excluded from the final model.

(XLSX)

S5 Table. F- and P-values from mixed linear models of gastrocnemius muscle capillarity and enzyme activity in *Epas1* variants of deer mice. n.s. not significant and excluded from the final model.

(XLSX)

S6 Table. F- and P-values from mixed linear models of ventilatory and metabolic responses of *Epas1* variants of deer mice. n.s. not significant and excluded from the final model.

(XLSX)

S7 Table. Candidate set of hypoxia inducible factor (HIF) cascade target genes and catecholamine synthesis and secretion genes used in targeted differential gene expression analysis. Candidate genes were curated from the literature (Ortiz-Barahona et al. 2010; Dengler et al. 2016) and publically available databases (KEGG: Kyoto Encyclopedia of Genes and Genomes; AmiGO).

(XLSX)

S8 Table. Results of differential gene expression among candidate HIF and catecholamine genes. Table reports average log₂ fold-change (logFC) in expression, average log₂ read counts per million (logCPM), and the F-value (F) from quasi-likelihood F tests, p-value, and false-discovery rate corrected p-value (FDR) of quasi-likelihood generalized linear models comparing expression between *Epas1*^{L/L} vs. *Epas1*^{H/H} and *Epas1*^{H/L} for adrenal and left ventricle tissues. Gene names are *Mus musculus* gene ids.

(XLSX)

S9 Table. Maximum likelihood parameter estimates and 95% confidence intervals (CI) for demographic model.

(XLSX)

S10 Table. Results from gProfiler for gene ontology enrichment of genes containing SNPs above the 99.9th percentile of the empirical distribution of PBS values. Only categories significant above a Benjamini-Hochberg false-discovery rate of 0.05 are included.

(XLSX)

S11 Table. The list of hypoxia-related genes used in this study. The list of genes was extracted from Zhang et al. (2014), then orthologs in *Mus musculus* and *Peromyscus maniculatus* were identified using DAVID and custom scripts.

(XLSX)

S12 Table. Hypoxia-related genes containing SNPs with PBS values above the 99.9th percentile of the empirical distribution. For each gene, the PBS value, genomic location, and percentile of the highest-ranking SNP is provided.

(XLSX)

S13 Table. *Epas1* primer sequences. Primers were used to amplify *Epas1* prior to restriction enzyme digest for screening of alternative alleles. Sequences are given 5' to 3'. See supplemental text for PCR reaction conditions.

(XLSX)

S1 Fig. Mean Depth of Coverage for 100 Exomes. Distribution of mean depth of coverage for 100 exome samples used in this study. The final set of quality-filtered sites consists of 5,182,530 high-quality bi-allelic variants sequenced at approximately 18X coverage. Red dashed vertical line indicates the mean.

(PDF)

S2 Fig. PCA of Three Focal Populations. Principal components analysis of Mount Evans (n = 48), Lincoln (n = 37), and California (n = 15) mice, based on genotypes from 296,196 exome-wide LD-pruned SNPs with no missing data.

(PDF)

S3 Fig. Population assignment made via *Admixture* for K = 2 to K = 3 for 100 individuals. A) *Admixture* was run on a set of 296,196 exome-wide LD-pruned SNPs with no missing data. Each vertical bar represents an individual, with the colors corresponding to proportion

assignment at each value of K. B) The lowest cross validation error rate was at $K = 1$; however, higher values of K are biologically meaningful and are therefore shown here.

(PDF)

S4 Fig. Density distribution of population branch statistic (PBS) values calculated for Mount Evans, using Lincoln and Merced populations as outgroups. The mean (green vertical dashed line), 99th (blue vertical dotted line), and 99.9th (red dash-dotted line) values of the empirical distribution are shown. Orange vertical lines indicate three outlier SNPs located in *Epas1*, with the rightmost line indicating the ^{Thr755^{Met}} SNP.

(PDF)

S5 Fig. PBS Values for exonic SNPs in *Epas1*. Manhattan plot of PBS values for all SNPs (black dots) located within all exons of *Epas1*. Exome-wide values for mean, 99%, and 99.9th percentile PBS values are shown, and three outlier SNPs above the 99.9th percentile located in *Epas1* are highlighted in orange. Pairwise linkage disequilibrium estimates (measured with the squared correlation coefficient, r^2) for each SNP pair are provided.

(PDF)

S6 Fig. Correlation between *Epas1*^H frequency and sampling elevation. Significant positive correlation of high-elevation allele frequency with sampled elevation, based on genotyping 23 populations.

(PDF)

S7 Fig. Clinal variation in two-locus HBB haplotype frequencies. Clinal variation for nine *P. maniculatus* populations sampled along a 4500 m altitudinal cline from the Great Plains of Nebraska to the Rocky Mountains in Colorado. Data from Storz et al. 2012 *Genetics*.

(PDF)

S8 Fig. Histological analysis of capillarity in the gastrocnemius muscle. Capillaries were identified by staining for alkaline phosphatase activity. The oxidative core (A,C,E) and the outer less oxidative region (B,D,F) of the muscle is shown for representative individuals possessing *Epas1*^{H/H} (A,B), *Epas1*^{H/L} (C,D), and *Epas1*^{L/L} (E,F) genotypes. All images are shown at the same scale, and the scale bar represents 100 μm .

(PDF)

S9 Fig. Statistical analysis of capillarity in the gastrocnemius muscle. There were no differences in capillarity in the gastrocnemius muscle between deer mice with different *Epas1* genotypes. Capillarity was quantified using the following measurements: A) capillaries per muscle fiber, B) capillary surface density, C) capillary density, and D) transverse muscle area per muscle fiber. Sample sizes: $n = 16$ *Epas1*^{H/H}, $n = 13$ *Epas1*^{H/L}, and $n = 4$ *Epas1*^{L/L} variants.

(PDF)

S10 Fig. Activity of oxidative enzymes in the gastrocnemius muscle. The activities of oxidative enzymes, i.e. A) cytochrome c oxidase (COX) and B) citrate synthase (CS) in the gastrocnemius muscle were similar between deer mice with different *Epas1* genotypes, but C) lactate dehydrogenase (LDH) activity appeared to be lower in mice that were homozygous for the highland *Epas1* variant. † Significant difference in a post-hoc comparison between only *Epas1*^{H/H} and *Epas1*^{H/L} genotypes. $n = 16$ *Epas1*^{H/H}, $n = 13$ *Epas1*^{H/L}, and $n = 4$ *Epas1*^{L/L} variants.

(PDF)

S11 Fig. Ventilatory response of deer mice with varying *Epas1* genotype. Deer mice with different *Epas1* genotypes exhibited similar ventilatory responses to increasingly severe levels of acute hypoxia. Ventilation was quantified via A) total ventilation, B) arterial oxygen

saturation, C) breathing frequency, and D) tidal volume. Sample sizes: $n = 26$ *Epas1*^{H/H}, $n = 13$ *Epas1*^{H/L}, and $n = 4$ *Epas1*^{L/L} variants.

(PDF)

S12 Fig. Response of O₂ consumption rate and body temperature under acute hypoxia.

Deer mice with different *Epas1* genotypes exhibited similar declines in A) O₂ consumption rate and B) body temperature in response to increasingly severe levels of acute hypoxia, and similar increases in C) ventilatory equivalent for O₂ and D) pulmonary O₂ extraction. Sample sizes: $n = 26$ *Epas1*^{H/H}, $n = 13$ *Epas1*^{H/L}, and $n = 4$ *Epas1*^{L/L} variants.

(PDF)

S13 Fig. Heart rate response according to *Epas1* genotype. Deer mice that were homozygous for the highland *Epas1* variant exhibited a significantly greater increase in heart rate from normoxia (21 kPa O₂) to environmentally realistic levels of hypoxia at 4300 m elevation (12 kPa O₂). Measurements were made using a MouseOx Plus collar. * A significant pairwise difference between *Epas1*^{H/H} and *Epas1*^{H/L} mice. $n = 26$ *Epas1*^{H/H}, $n = 13$ *Epas1*^{H/L}, and $n = 4$ *Epas1*^{L/L} variants.

(PDF)

S14 Fig. Results of demographic modeling in deer mice. The folded 2-dimensional site frequency spectra (2d-SFS) for deer mice from (A) Mt. Evans, CO, and Merced, CA, and (B) Mt. Evans, CO, and Lincoln, NE. For each pair of populations, we show the empirical 2d-SFS from whole exome data and the maximum likelihood 2d-SFS for demographic models with no migration, one migration rate, and two migration rates. Residuals reflect the overall fit of the model to the empirical data, where red indicates an overestimation of the number of SNPs by the model and blue reflects an underestimation.

(PDF)

S15 Fig. Density distributions of PBS values under simulated and empirical models. A)

Density plot of population branch statistic (PBS) values calculated for Mount Evans, using Lincoln and Merced populations as outgroups, from 10,000 SNPs simulated under modeled demography. Values for the mean (green vertical dashed line), 99th (blue vertical dotted line), and 99.9th (red dash-dotted line) percentiles of the simulated distribution are shown. B) Density plot of empirical PBS values (same as in S4 Fig), but with significance thresholds based on simulated 99th and 99.9th percentile shown.

(PDF)

Acknowledgments

We thank Kamilla Bentsen for help extracting RNA, and Jean-Marc Lassance and Hopi Hoekstra for providing access to *Peromyscus maniculatus* genome liftover files. We thank Michael Nachman and Erica Rosenblum for sharing previously unpublished data. Tissue samples were kindly loaned by the Museum of Southwestern Biology (2017.044.Mamm), Museum of Comparative Zoology (2017-56-Cryo), and the Museum of Vertebrate Zoology.

Author Contributions

Conceptualization: Rena M. Schweizer, Jonathan P. Velotta, Graham R. Scott, Zachary A. Cheviron.

Data curation: Rena M. Schweizer, Jonathan P. Velotta, Catherine M. Ivy, Sarah M. Muir, Gideon S. Bradburd, Jay F. Storz, Graham R. Scott, Zachary A. Cheviron.

Formal analysis: Rena M. Schweizer, Jonathan P. Velotta, Catherine M. Ivy, Matthew R. Jones, Sarah M. Muir, Graham R. Scott, Zachary A. Cheviron.

Funding acquisition: Rena M. Schweizer, Jonathan P. Velotta, Catherine M. Ivy, Jay F. Storz, Graham R. Scott, Zachary A. Cheviron.

Investigation: Rena M. Schweizer, Jonathan P. Velotta, Catherine M. Ivy, Matthew R. Jones, Sarah M. Muir, Gideon S. Bradburd, Jay F. Storz, Graham R. Scott, Zachary A. Cheviron.

Resources: Gideon S. Bradburd, Graham R. Scott, Zachary A. Cheviron.

Visualization: Rena M. Schweizer, Jonathan P. Velotta, Catherine M. Ivy, Matthew R. Jones.

Writing – original draft: Rena M. Schweizer, Jonathan P. Velotta, Catherine M. Ivy, Matthew R. Jones, Graham R. Scott, Zachary A. Cheviron.

Writing – review & editing: Rena M. Schweizer, Jonathan P. Velotta, Catherine M. Ivy, Matthew R. Jones, Sarah M. Muir, Gideon S. Bradburd, Jay F. Storz, Graham R. Scott, Zachary A. Cheviron.

References

1. Storz JF, Bridgham JT, Kelly SA, Garland T Jr. Genetic approaches in comparative and evolutionary physiology. *American Journal of Physiology- Regulatory, Integrative and Comparative Physiology*. 2015; 309: R197–R214. <https://doi.org/10.1152/ajpregu.00100.2015> PMID: 26041111
2. Wagner A. Metabolic networks and their evolution. Soyer OS, editor. *Evolutionary Systems Biology*. 2012;: 29–52. <https://doi.org/10.1007/978-1-4614-3567-9>
3. Wagner GP, Lynch VJ. The gene regulatory logic of transcription factor evolution. *Trends in Ecology & Evolution*. 2008; 23: 377–385. <https://doi.org/10.1016/j.tree.2008.03.006> PMID: 18501470
4. Lynch VJ, Wagner GP. Resurrecting the role of transcription factor change in developmental evolution. *Evolution*. 2008; 62: 2131–2154. <https://doi.org/10.1111/j.1558-5646.2008.00440.x> PMID: 18564379
5. Stern DL, Orgogozo V. Is Genetic Evolution Predictable? *Science*. American Association for the Advancement of Science; 2009; 323: 746–751. <https://doi.org/10.1126/science.1158997> PMID: 19197055
6. Carroll SB. Evo-Devo and an Expanding Evolutionary Synthesis: A Genetic Theory of Morphological Evolution. *Cell*. 2008; 134: 25–36. <https://doi.org/10.1016/j.cell.2008.06.030> PMID: 18614008
7. Bouverot P. Adaptation to altitude-hypoxia in vertebrates. 1985. Springer Science & Business Media, Berlin, Germany.
8. Beall CM, Cavalleri GL, Deng L. Natural selection on EPAS1 (HIF2 α) associated with low hemoglobin concentration in Tibetan highlanders. *Proc Natl Acad Sci*. 2010; 107: 11459–11464. <https://doi.org/10.1073/pnas.1002443107> PMID: 20534544
9. Scott GR, Milsom WK. Control of breathing and adaptation to high altitude in the bar-headed goose. *American Journal of Physiology- Regulatory, Integrative and Comparative Physiology*. 2007; 293: R379–R391. <https://doi.org/10.1152/ajpregu.00161.2007> PMID: 17491113
10. Storz JF, Scott GR, Cheviron ZA. Phenotypic plasticity and genetic adaptation to high-altitude hypoxia in vertebrates. *J Exp Biol*. 2010; 213: 4125–4136. <https://doi.org/10.1242/jeb.048181> PMID: 21112992
11. Semenza GL. Hypoxia-inducible factor 1: oxygen homeostasis and disease pathophysiology. *Trends in Molecular Medicine*. 2001; 7:345–350. PMID: 11516994
12. Simonson TS, Yang Y, Huff CD, Yun H, Qin G, Witherspoon DJ, et al. Genetic Evidence for High-Altitude Adaptation in Tibet. *Science*. 2010; 329: 72–75. <https://doi.org/10.1126/science.1189406> PMID: 20466884
13. Yi X, Liang Y, Huerta-Sanchez E, Jin X, Cuo ZXP, Pool JE, et al. Sequencing of 50 Human Exomes Reveals Adaptation to High Altitude. *Science*. 2010; 329: 75–78. <https://doi.org/10.1126/science.1190371> PMID: 20595611
14. Zhang W, Fan Z, Han E, Hou R, Zhang L, Galaverni M, et al. Hypoxia Adaptations in the Grey Wolf (*Canis lupus chanco*) from Qinghai-Tibet Plateau. *PLoS Genet*. 2014; 10: e1004466. <https://doi.org/10.1371/journal.pgen.1004466> PMID: 25078401
15. Pan S, Zhang T, Rong Z, Hu L, Gu Z, Wu Q, et al. Population transcriptomes reveal synergistic responses of DNA polymorphism and RNA expression to extreme environments on the Qinghai-Tibetan

- Plateau in a predatory bird. *Molecular Ecology*. 2017; 26: 2993–3010. <https://doi.org/10.1111/mec.14090> PMID: 28277617
16. Hodson EJ, Nicholls LG, Turner PJ, Llyr R, Fielding JW, Douglas G, et al. Regulation of ventilatory sensitivity and carotid body proliferation in hypoxia by the PHD2/HIF-2 pathway. *J Physiol*. 2015; 594: 1179–1195. <https://doi.org/10.1113/JP271050> PMID: 26337139
 17. Befani C, Liakos P. The role of hypoxia-inducible factor-2 alpha in angiogenesis. *J Cell Physiol*. 2018; 233: 9087–9098. <https://doi.org/10.1002/jcp.26805> PMID: 29968905
 18. Petousi N, Croft QPP, Cavalleri GL, Cheng H-Y, Formenti F, Ishida K, et al. Tibetans living at sea level have a hyporesponsive hypoxia-inducible factor system and blunted physiological responses to hypoxia. *Journal of Applied Physiology*. 2014; 116: 893–904. <https://doi.org/10.1152/jappphysiol.00535.2013> PMID: 24030663
 19. Lorenzo FR, Huff C, Myllymäki M, Olenchock B, Swierczek S, Tashi T, et al. A genetic mechanism for Tibetan high-altitude adaptation. *Nature*. 2014; 46: 951–956. <https://doi.org/10.1038/ng.3067> PMID: 25129147
 20. Fielding JW, Hodson EJ, Cheng X, Ferguson DJP, Eckardt L, Adam J, et al. PHD2 inactivation in Type I cells drives HIF-2 α -dependent multilineage hyperplasia and the formation of paraganglioma-like carotid bodies. *J Physiol*. 2018; 596: 4393–4412. <https://doi.org/10.1113/JP275996> PMID: 29917232
 21. Brown ST, Kelly KF, Daniel JM, Nurse CA. Hypoxia inducible factor (HIF)-2 α is required for the development of the catecholaminergic phenotype of sympathoadrenal cells. *Journal of Neurochemistry*. 2009; 110: 622–630. <https://doi.org/10.1111/j.1471-4159.2009.06153.x> PMID: 19457096
 22. Cowburn AS, Crosby A, Macias D, Branco C, Colaço RDDR, Southwood M, et al. HIF2 α -arginase axis is essential for the development of pulmonary hypertension. *PNAS*. 2016; 113: 8801–8806. <https://doi.org/10.1073/pnas.1602978113> PMID: 27432976
 23. Chappell MA, Snyder LR. Biochemical and physiological correlates of deer mouse alpha-chain hemoglobin polymorphisms. *PNAS*. 1984; 81: 5484–5488. <https://doi.org/10.1073/pnas.81.17.5484> PMID: 6591201
 24. Cheviron ZA, Bachman GC, Storz JF. Contributions of phenotypic plasticity to differences in thermogenic performance between highland and lowland deer mice. *J Exp Biol*. 2013; 216: 1160–1166. <https://doi.org/10.1242/jeb.075598> PMID: 23197099
 25. Cheviron ZA, Bachmana GC, Connaty AD, McClelland GB, Storz JF. Regulatory changes contribute to the adaptive enhancement of thermogenic capacity in high-altitude deer mice. *PNAS*. 2012; 109: 8635–8640. <https://doi.org/10.1073/pnas.1120523109> PMID: 22586089
 26. Scott GR, Elogio TS, Lui MA, Storz JF, Cheviron ZA. Adaptive Modifications of Muscle Phenotype in High-Altitude Deer Mice Are Associated with Evolved Changes in Gene Regulation. *Molecular Biology and Evolution*. 2015; 32: 1962–1976. <https://doi.org/10.1093/molbev/msv076> PMID: 25851956
 27. Hayes J, O'Connor C. Natural selection on thermogenic capacity of high-altitude deer mice. *Evolution*. 1999; 53: 1280–1287. <https://doi.org/10.1111/j.1558-5646.1999.tb04540.x> PMID: 28565539
 28. Storz JF, Runck AM, Moriyama H, Weber RE, Fago A. Genetic differences in hemoglobin function between highland and lowland deer mice. *J Exp Biol*. 2010; 213: 2565–2574. <https://doi.org/10.1242/jeb.042598> PMID: 20639417
 29. Snyder LRG. Deer Mouse Hemoglobins: Is There Genetic Adaptation to High Altitude? *BioScience*. 1981; 31: 299–304. <https://doi.org/10.2307/1308147>
 30. Snyder LR, Born S, Lechner AJ. Blood oxygen affinity in high- and low-altitude populations of the deer mouse. *Respir Physiol*. 1982; 48: 89–105. [https://doi.org/10.1016/0034-5687\(82\)90052-4](https://doi.org/10.1016/0034-5687(82)90052-4) PMID: 7111920
 31. Cheviron ZA, Connaty AD, McClelland GB, Storz JF. Functional genomics of adaptation to hypoxic cold-stress in high-altitude deer mice: transcriptomic plasticity and thermogenic performance. *Evolution*. 2014; 68: 48–62. <https://doi.org/10.1111/evo.12257> PMID: 24102503
 32. Lui MA, Mahalingam S, Patel P, Connaty AD, Ivy CM, Cheviron ZA, et al. High-altitude ancestry and hypoxia acclimation have distinct effects on exercise capacity and muscle phenotype in deer mice. *American Journal of Physiology- Regulatory, Integrative and Comparative Physiology*. 2015; 308: R779–R791. <https://doi.org/10.1152/ajpregu.00362.2014> PMID: 25695288
 33. Velotta JP, Jones J, Wolf CJ, Cheviron ZA. Transcriptomic plasticity in brown adipose tissue contributes to an enhanced capacity for nonshivering thermogenesis in deer mice. *Molecular Ecology*. 2016; 25: 2870–2886. <https://doi.org/10.1111/mec.13661> PMID: 27126783
 34. Ivy CM, Scott GR. Control of breathing and ventilatory acclimatization to hypoxia in deer mice native to high altitudes. *Acta Physiol*. 1st ed. 2017; 112: 123–17. <https://doi.org/10.1111/apha.12912> PMID: 28640969

35. Tate KB, Ivy CM, Velotta JP, Storz JF, McClelland GB, Cheviron ZA, et al. Circulatory mechanisms underlying adaptive increases in thermogenic capacity in high-altitude deer mice. *Journal of Experimental Biology*. 2017; 220: 3616–3620. <https://doi.org/10.1242/jeb.164491> PMID: 28839010
36. Velotta JP, Ivy CM, Wolf CJ, Scott GR, Cheviron ZA. Maladaptive phenotypic plasticity in cardiac muscle growth is suppressed in high-altitude deer mice. *Evolution*. 2018; 431: 261–16. <https://doi.org/10.1111/evo.13626> PMID: 30318588
37. Dawson NJ, Lyons SA, Henry DA, Scott GR. Effects of chronic hypoxia on diaphragm function in deer mice native to high altitude. *Acta Physiol*. 2018; 223: e13030–16. <https://doi.org/10.1111/apha.13030> PMID: 29316265
38. Mahalingam S, McClelland GB, Scott GR. Evolved changes in the intracellular distribution and physiology of muscle mitochondria in high-altitude native deer mice. *J Physiol*. 2017; 595: 4785–4801. <https://doi.org/10.1113/JP274130> PMID: 28418073
39. Lau DS, Connaty AD, Mahalingam S, Wall N, Cheviron ZA, Storz JF, et al. Acclimation to hypoxia increases carbohydrate use during exercise in high-altitude deer mice. *American Journal of Physiology-Regulatory, Integrative and Comparative Physiology*. 2017; 312: R400–R411. <https://doi.org/10.1152/ajpregu.00365.2016> PMID: 28077391
40. Purcell S, Neale B, Todd-Brown K, Thomas L, Ferreira MAR, Bender D, et al. PLINK: a tool set for whole-genome association and population-based linkage analyses. *Am J Hum Genet*. 2007; 81: 559–575. <https://doi.org/10.1086/519795> PMID: 17701901
41. Alexander D, Novembre J, Lange K. Fast model-based estimation of ancestry in unrelated individuals. *Genome Research*. 2009; 19: 1655. <https://doi.org/10.1101/gr.094052.109> PMID: 19648217
42. Weir B, Cockerham C. Estimating F-statistics for the analysis of population structure. *Evolution*. 1984; 38: 1358–1370. <https://doi.org/10.1111/j.1558-5646.1984.tb05657.x> PMID: 28563791
43. Storz JF, Natarajan C, Cheviron ZA, Hoffmann FG, Kelly JK. Altitudinal Variation at Duplicated -Globin Genes in Deer Mice: Effects of Selection, Recombination, and Gene Conversion. *Genetics*. 2012; 190: 203–216. <https://doi.org/10.1534/genetics.111.134494> PMID: 22042573
44. Pugh CW, Ratcliffe PJ. Regulation of angiogenesis by hypoxia: role of the HIF system. *Nat Med*. 2003; 9: 677–684. <https://doi.org/10.1038/nm0603-677> PMID: 12778166
45. Lohman BK, Weber JN, Bolnick DI. Evaluation of TagSeq, a reliable low-cost alternative for RNAseq. *Mol Ecol Resour*. 2016; 16: 1315–1321. <https://doi.org/10.1111/1755-0998.12529> PMID: 27037501
46. Scott AL, Pranckevicius NA, Nurse CA, Scott GR. The regulation of catecholamine release from the adrenal medulla is altered in deer mice (*Peromyscus maniculatus*) native to high altitudes. *American Journal of Physiology-Regulatory, Integrative and Comparative Physiology*. 2019; 584: 149–R417. <https://doi.org/10.1152/ajpregu.00005.2019>
47. Hamid SA, Baxter GF. Adrenomedullin: regulator of systemic and cardiac homeostasis in acute myocardial infarction. *Pharmacology & Therapeutics*. 2005; 105: 95–112. <https://doi.org/10.1016/j.pharmthera.2004.08.012> PMID: 15670621
48. Bohm F, Pernow J. The importance of endothelin-1 for vascular dysfunction in cardiovascular disease. *Cardiovascular Research*. 2007; 76: 8–18. <https://doi.org/10.1016/j.cardiores.2007.06.004> PMID: 17617392
49. Song W, Wang H, Wu Q. Atrial natriuretic peptide in cardiovascular biology and disease (NPPA). *Gene*. 2015; 569: 1–6. <https://doi.org/10.1016/j.gene.2015.06.029> PMID: 26074089
50. Gutenkunst R, Hernandez R, Williamson S, Bustamante C. Inferring the joint demographic history of multiple populations from multidimensional SNP frequency data. *PLoS Genet*. 2009; 5: e1000695. <https://doi.org/10.1371/journal.pgen.1000695> PMID: 19851460
51. Tine M, Kuhl H, Gagnaire P-A, Louro B, Desmarais E, Martins RST, et al. European sea bass genome and its variation provide insights into adaptation to euryhalinity and speciation. *Nature Communications*. 2014; 5: 1–10. <https://doi.org/10.1038/ncomms6770> PMID: 25534655
52. Coffman AJ, Hsieh PH, Gravel S. Computationally efficient composite likelihood statistics for demographic inference. *Molecular Biology and Evolution*. 2016. <https://doi.org/10.1093/molbev/msv255/-/DC1>
53. Ewing G, Hermisson J. MSMS: a coalescent simulation program including recombination, demographic structure and selection at a single locus. *Bioinformatics*. 2010; 26: 2064–2065. <https://doi.org/10.1093/bioinformatics/btq322> PMID: 20591904
54. Mayer U, Saher G, Fässler R, Bornemann A, Echtermeyer F, Mark von der H, et al. Absence of integrin alpha 7 causes a novel form of muscular dystrophy. *Nat Genet*. 1997; 17: 318–323. <https://doi.org/10.1038/ng1197-318> PMID: 9354797
55. Tomás M, Vázquez E, Fernández-Fernández JM, Subirana I, Plata C, Heras M, et al. Genetic variation in the KCNMA1 potassium channel α subunit as risk factor for severe essential hypertension and

- myocardial infarction. *Journal of Hypertension*. 2008; 26: 2147–2153. <https://doi.org/10.1097/HJH.0b013e32831103d8> PMID: 18854754
56. Harned J, Ferrell J, Nagar S, Goralska M, Fleisher LN, McGahan MC. Ceruloplasmin alters intracellular iron regulated proteins and pathways: Ferritin, transferrin receptor, glutamate and hypoxia-inducible factor-1 α . *Experimental Eye Research*. 2012; 97: 90–97. <https://doi.org/10.1016/j.exer.2012.02.001> PMID: 22343016
 57. Simonson TS, Yang Y, Huff CD, Yun H, Qin G. Genetic evidence for high-altitude adaptation in Tibet. *Science*. 2010; 329: 72–75. <https://doi.org/10.1126/science.1189406> PMID: 20466884
 58. Liu X, Zhang Y, Li Y, Pan J, Wang D, Chen W, et al. EPAS1 gain-of-function mutation contributes to high-altitude adaptation in Tibetan horses. *Molecular Biology and Evolution*. 2019; 19: 1655. <https://doi.org/10.1093/molbev/msz158> PMID: 31273382
 59. Julian CG, Moore LG. Human Genetic Adaptation to High Altitude: Evidence from the Andes. *Genes*. 2019; 10: 150–21. <https://doi.org/10.3390/genes10020150> PMID: 30781443
 60. Nelson TC, Jones MR, Velotta JP, Dhawanjewar AS, Schweizer RM. UNVEILING connections between genotype, phenotype, and fitness in natural populations. *Molecular Ecology*. 2019; 28: 1–31. <https://doi.org/10.1111/mec.14976>
 61. Dempsey JA, Morgan BJ. Humans In Hypoxia: A Conspiracy Of Maladaptation?! *Physiology*. 2015; 30: 304–316. <https://doi.org/10.1152/physiol.00007.2015> PMID: 26136544
 62. Wu T, Kayser B. High altitude adaptation in Tibetans. *High Altitude Medicine & Biology*. 2006; 7: 193–208. <https://doi.org/10.1089/ham.2006.7.193> PMID: 16978132
 63. Meyer M, Kircher M. Illumina Sequencing Library Preparation for Highly Multiplexed Target Capture and Sequencing. *Cold Spring Harbor Protocols*. 2010. <https://doi.org/10.1101/pdb.prot5448> PMID: 20516186
 64. Li H, Durbin R. Fast and accurate long-read alignment with Burrows-Wheeler transform. *Bioinformatics*. 2010; 26: 589–595. <https://doi.org/10.1093/bioinformatics/btp698> PMID: 20080505
 65. Li H, Handsaker B, Wysoker A, Fennell T, Ruan J, Homer N, et al. The Sequence Alignment/Map format and SAMtools. *Bioinformatics*. 2009; 25: 2078–2079. <https://doi.org/10.1093/bioinformatics/btp352> PMID: 19505943
 66. Danecek P, Auton A, Abecasis G, Albers CA, Banks E, DePristo MA, et al. The variant call format and VCFtools. *Bioinformatics*. 2011; 27: 2156–2158. <https://doi.org/10.1093/bioinformatics/btr330> PMID: 21653522
 67. McLaren W, Pritchard B, Rios D, Chen Y, Flicek P, Cunningham F. Deriving the consequences of genomic variants with the Ensembl API and SNP Effect Predictor. *Bioinformatics*. 2010; 26: 2069–2070. <https://doi.org/10.1093/bioinformatics/btq330> PMID: 20562413
 68. Bradley R, Durish ND, Rogers DS, Miller JR, Engstrom MD, Kilpatrick CW. Toward a molecular phylogeny for *Peromyscus*: evidence from mitochondrial cytochrome-b sequences. *Journal of Mammalogy*. 2007; 88: 1146–1159. <https://doi.org/10.1644/06-MAMM-A-342R.1> PMID: 19924266
 69. Miller JR, Engstrom MD. The Relationships of Major Lineages within Peromyscine Rodents: A Molecular Phylogenetic Hypothesis and Systematic Reappraisal. *Journal of Mammalogy*. 2008; 89: 1279–1295. <https://doi.org/10.2307/25145219>
 70. Natarajan C, Hoffmann FG, Lanier HC, Wolf CJ, Cheviron ZA, Spangler ML, et al. Intraspecific Polymorphism, Interspecific Divergence, and the Origins of Function-Altering Mutations in Deer Mouse Hemoglobin. *Molecular Biology and Evolution*. 2015; 32: 978–997. <https://doi.org/10.1093/molbev/msu403> PMID: 25556236
 71. Derryberry EP, Derryberry GE, Maley JM, Brumfield RT. hzar: hybrid zone analysis using an R software package. *Mol Ecol Resour*. 2013; 14: 652–663. <https://doi.org/10.1111/1755-0998.12209> PMID: 24373504
 72. Ivy CM, Scott GR. Ventilatory acclimatization to hypoxia in mice: Methodological considerations. *Respiratory Physiology & Neurobiology*. 2017; 235: 95–103. <https://doi.org/10.1016/j.resp.2016.10.012> PMID: 27989891
 73. Lighton JR. *Measuring Metabolic Rates: A Manual for Scientists*: Oxford University Press. 2008.
 74. Rosenmann M, Morrison P. Maximum oxygen consumption and heat loss facilitation in small homeotherms by He-O₂. *Am J Physiol*. 1974; 226: 490–495. <https://doi.org/10.1152/ajplegacy.1974.226.3.490> PMID: 4817400
 75. Scherle W. A simple method for volumetry of organs in quantitative stereology. *Mikroskopie*. 1970; 26: 57–60. PMID: 5530651

76. Nikel KE, Shanishchara NK, Ivy CM, Dawson NJ, Scott GR. Effects of hypoxia at different life stages on locomotory muscle phenotype in deer mice native to high altitudes. *Comparative Biochemistry and Physiology, Part B*. 2017; 224: 98–104. <https://doi.org/10.1016/j.cbpb.2017.11.009> PMID: 29175484
77. Schneider CA, Rasband WS, Eliceiri KW. NIH Image to ImageJ: 25 years of image analysis. *Nat Methods*. 2012; 9: 671–675. <https://doi.org/10.1038/nmeth.2089> PMID: 22930834
78. Liao Y, Smyth GK, Shi W. featureCounts: an efficient general purpose program for assigning sequence reads to genomic features. *Bioinformatics*. 2014; 30: 923–930. <https://doi.org/10.1093/bioinformatics/btt656> PMID: 24227677
79. Robinson MD, Smyth GK. Moderated statistical tests for assessing differences in tag abundance. *Bioinformatics*. 2007; 23: 2881–2887. <https://doi.org/10.1093/bioinformatics/btm453> PMID: 17881408
80. Robinson MD, Oshlack A. A scaling normalization method for differential expression analysis of RNA-seq data. *Genome Biology*. 2010; 11: R25. <https://doi.org/10.1186/gb-2010-11-3-r25> PMID: 20196867
81. McCarthy DJ, Chen Y, Smyth GK. Differential expression analysis of multifactor RNA-Seq experiments with respect to biological variation. *Nucleic Acids Research*. 2012; 40: 4288–4297. <https://doi.org/10.1093/nar/gks042> PMID: 22287627
82. Benjamini Y, Hochberg Y. Controlling the false discovery rate: a practical and powerful approach to multiple testing. *Journal of the Royal Statistical Society*. 1995; 57: 289–300.
83. Dengler VL, Galbraith MD, Espinosa JM. Transcriptional regulation by hypoxia inducible factors. *Critical Reviews in Biochemistry and Molecular Biology*. 2014; 49: 1–15. <https://doi.org/10.3109/10409238.2013.838205> PMID: 24099156
84. Ortiz-Barahona A, Villar D, Pescador N, Amigo J, del Peso L. Genome-wide identification of hypoxia-inducible factor binding sites and target genes by a probabilistic model integrating transcription-profiling data and in silico binding site prediction. *Nucleic Acids Research*. 2010; 38: 2332–2345. <https://doi.org/10.1093/nar/gkp1205> PMID: 20061373
85. Kanehisa M, Goto S. KEGG: kyoto encyclopedia of genes and genomes. *Nucleic Acids Research*. 2000; 28: 27–30. <https://doi.org/10.1093/nar/28.1.27> PMID: 10592173
86. Uchimura A, Higuchi M, Minakuchi Y, Ohno M, Toyoda A, Fujiyama A, et al. Germline mutation rates and the long-term phenotypic effects of mutation accumulation in wild-type laboratory mice and mutator mice. *Genome Research*. 2015; 25: 1125–1134. <https://doi.org/10.1101/gr.186148.114> PMID: 26129709
87. Reimand J, Arak T, Adler P, Kolberg L, Reisberg S, Peterson H, et al. g:Profiler—a web server for functional interpretation of gene lists (2016 update). *Nucleic Acids Research*. 2016;: gkw199. <https://doi.org/10.1093/nar/gkw199> PMID: 27098042